

## Geological Characteristics and Ore-controlling Factors of the Beiya Gold–Polymetallic Ore Deposit, Northwestern Yunnan Province

ZHOU Yunman<sup>1</sup>, ZHANG Changqing<sup>2,\*</sup>, HE Zhonghua<sup>1</sup>, LIU Huan<sup>2</sup>,  
ZHOU Guiwu<sup>1</sup>, SUN Jia<sup>2</sup> and LIU Bo<sup>3</sup>

<sup>1</sup> Yunnan Gold & Mining Group Co. Ltd., Kunming 650224, China

<sup>2</sup> MNR Key Laboratory of Metallogeny and Mineral Assessment, Institute of Mineral Resources, Chinese Academy of Geological Sciences, Beijing 100037, China

<sup>3</sup> Beijing Research Institute of Uranium Geology, Beijing 100029, China

**Abstract:** Based on comprehensive petrological, geochronological, and geochemical studies, this study analyzed the relationships between the Beiya gold-polymetallic skarn deposit and quartz syenite porphyries, and discussed the source(s) and evolution of magmas. Our results suggest that syenite porphyries (i.e. the Wandongshan, the Dashadi, and the Hongnitang porphyries), which formed between the Eocene and the early Oligocene epochs, are the sources for the gold-polymetallic ores at the Beiya deposit. Carbonate rocks (T<sub>2b</sub>) of the Triassic Beiya Formation in the ore district provide favorable host space for deposit formation. Fold and fault structures collectively play an important role in ore formation. The contact zone between the porphyries and carbonates, the structurally fractured zone of carbonate and clastic rocks, and the zone with well-developed fractures are the ideal locations for ore bodies. Four types of mineralization have been recognized: 1) porphyry-style stockwork gold–iron (copper) ore, 2) skarn-style gold-iron (copper and lead) ore in the near contact zone, 3) strata-bound, lense-type lead–silver–gold ore in the outer contact zone, and 4) distal vein-type gold–lead–silver ore. Supergene processes led to the formation of oxide ore, such as the weathered and accumulated gold–iron ore, the strata-bound fracture oxide ore, and the structure-controlled vein-type ore. Most of these ore deposits are distributed along the axis of the depressed basin, with the hypogene ore controlling the shape and characteristics of the oxide ore. This study provides critical geology understanding for mineral prospecting scenarios.

**Key words:** porphyry-skarn type, quartz syenite porphyries, ore-controlling factors, Beiya gold–polymetallic deposit, northwestern Yunnan province

### 1 Introduction

The Beiya ore deposit is a super large porphyry-skarn gold polymetallic deposit discovered by Yunnan Gold & Mining Group Co., Ltd., and has been explored continuously throughout the past 10 years. Several previous studies have been conducted in the Beiya deposit, which provide important data about geological characteristics, rock types and distribution, rock-forming and ore-forming ages of porphyries and ores, and deposit genesis in the Beiya gold field, as well as ore deposit and prospecting models, prospecting methods and predictions (Cai Xinping et al., 1991; Cai Xinping, 1993; Chen Aibin

et al., 2011; Cui Yinliang et al., 2001, 2003; Deng Jun et al., 2010, 2012; Ge Liangsheng et al., 2002; Li Jinghong et al., 1991; Ma Deyun and Han Runsheng, 2001; Fu Weimin and Hu Chaoping, 1994; Ren Zhiji et al., 2001; Song Huanbin and He Mingqin, 1994; Wu Kaixing et al., 2005; Xiao Qibin et al., 2003; Xiao Xiaoniu et al., 2009a, 2009b, 2011; Xu Shouming et al., 2006; Xu Xingwang et al., 2006, 2007; Yan Jianguo et al., 2002, 2003; Xue Chuandong et al., 2008; Yang Shiyu and Wang Rixue, 2002; Ying Hanlong and Cai Xinping, 2004; Zhong Kunming and Yang Shiyu, 2000; Zou Guangfu et al., 2013). In recent years, a scientific research team, organized by Yunnan Gold & Mining Group, has carried out “Three-in-One” prospecting prediction research in the Beiya gold-polymetallic ore exploration area (He Wenyan

\* Corresponding author. E-mail: zcchangqing@163.com

et al., 2012, 2013; He Wenyan, 2014; He et al., 2014; 2015; He Zhonghua et al., 2013, 2014, 2016; Jia Ruya et al., 2016; Jiang Wentao et al., 2015; Deng et al., 2015a; ; 2015b; Fu et al., 2015; 2016; Zhou et al., 2016; Li et al., 2016; Liu Fei et al., 2016; Mao et al., 2017; Niu Haobin et al., 2015; Wang Jianhua et al., 2015, 2016; Wang Mingzhi et al., 2016; Li and Wang, 2014; Li et al., 2016; Yang Jian et al., 2014, 2015; Zhou Yunman et al., 2013, 2014, 2015, 2016, 2017). Based on previous study results and intensive geological investigation in this study, this paper analyzed key metallogenic geological processes and ore-controlling factors and clarified prospecting directions and target orebodies in the ore district and its peripheries, by carrying out geochemical analysis of alkali-rich porphyry intrusive bodies and zircon dating for quartz syenite and quartz monzonite porphyry samples from several ore sections. Therefore, this study is of some significance for better understanding the ore-controlling factors and ore-forming mechanism of this deposit.

## 2 Geological Backgrounds

### 2.1 Regional geology

Located on the northeastern side of Jinsha River–Ailaoshan–Red River strike slip fault, the Beiya superlarge gold ore deposit is an archetype deposit within the large Tethys porphyry-skarn-type copper polymetallic metallogenic belt (Hou et al., 2007; Mao et al., 2014), and formed by the decomposition of an oblique collision between the southeastern Indian continental margin and the Asian continent (Xu Zhiqin, 2011). The deposit geotectonically belongs to the Heqing terrace ( $T_{2-3}$ )–Songgui faulted basin ( $T_3$ ) in the central region of the Yanyuan–Lijiang passive continental margin rift basin ( $P_2$ ) along the western margin of the Yangtze block. Structurally controlled by the NNW Jinsha River–Red River fault, the NE Binchuan–Chenghai fault, as well as the Lijiang–Muli fault, the Beiya deposit, the Beiya deposit belongs to intermountane basin adjacent to the Zhongzan–Zhongdian massif to the northwest and the Jinsha River–Ailaoshan combined belt to the west (Pan Guitang, 2009). This region is composed of the upper Sinian and Cambrian series (e.g., magnesian carbonate rock and sandy-argillaceous formations) as well as Ordovician to middle Triassic series (e.g., littoral neritic carbonate rocks and sandy-argillaceous formations). Between the Indosinian and Yanshanian periods, the entire region experienced uplift, causing Minssing the Jurassic–Cretaceous series. From the Eocene to the beginning of the Neogene, molasse and coal-bearing formations accumulated in the mountain basin. The overall regional structure is characterized by south-to-north trends, with

the Heqing–Songgui–Beiya open compound syncline and Ma'anshan fault as the main structural components of the region. The Beiya syncline belongs to the secondary syncline of the Heqing–Songgui–Beiya compound syncline. Regional alkali-rich porphyries, Cenozoic in age, are distributed along both sides of the Ailao Mountain–Jinsha River tectonic belt, and the ore district is located in the Heqing–Xiangyun alkali-rich porphyry zone in the middle of the belt. This zone is a part of the Heqing–Dali metallogenic subzone within the transition zone between the southwestern Sanjiang metallogenic belt and the Yangtze metallogenic belt (Gao Lan et al., 2016).

### 2.2 Geological characteristics of the deposit

Exposed strata in the region comprise upper Permian basalt Formations ( $P_2\beta$ ; intercalated basaltic tuff), the Lower Triassic Qingtianbao Formation ( $T_1q$ ; sandy conglomerate and sandstone), the Middle Triassic Beiya Formation ( $T_2b$ ; argillaceous limestone and dolomite), the Pliocene Sanying formation ( $N_2s$ ; sandy conglomerate and claystone), and Holocene clay ( $Q_4$ ). The ore district is oriented southnorthly (i.e. a wide-flat short axis syncline) where strata from the  $T_2b^{1-5}$  are exposed in the west limb, and strata from the  $T_2b^{1-5}$ ,  $T_1q$ , and  $P_2\beta$  are exposed in the east limb. The strata at the core are gentle and give the northsouth-trending intermountain basin its geomorphological characteristics. Four sets of faults exist in the orientation of southnorth (SN), eastwest (EW), northwest (NW), and northeast (NE). Faults oriented in SN are F1–F6; EW faults mainly have F22, F25, and F26; NW faults are mainly F21 and F28; and NE faults are mainly F23 and F27 (Fig. 1). Magmatic rocks are dominantly Himalayan alkali-rich porphyries. The rock body is dominated by quartz syenite porphyry, followed by syenite porphyry, with biotite quartz syenite porphyry and lamprophyre veins throughout the region.

The ore district contains both hypogene and supergene mineralization types, with the former being important in reserves. Hypogene mineralization mainly occurs in the alkali-rich porphyry and  $T_2b$  carbonate rocks. The porphyry-skarn-type ore bodies, in the exocontact zone, are distributed in a ring pattern around the rock body, and their occurrences synchronously change with the contact zone of the rock body. The supergene mineralization occurs in  $N_2s$  and weathering-accumulation type ore bodies along the unconformity above the  $T_2b$  and the porphyry body. According to shape and spatial position, the porphyry-skarn-type ore bodies can be divided into four sub-types: 1) an Fe–Au (Cu/Mo) ore body hosted in steep fissures occurring as lenticulars and veins in the alkali-rich porphyry; 2) an Fe–Au–Cu–Pb or Fe–Cu (Mo) ore body hosted in skarns occurring as block shape and

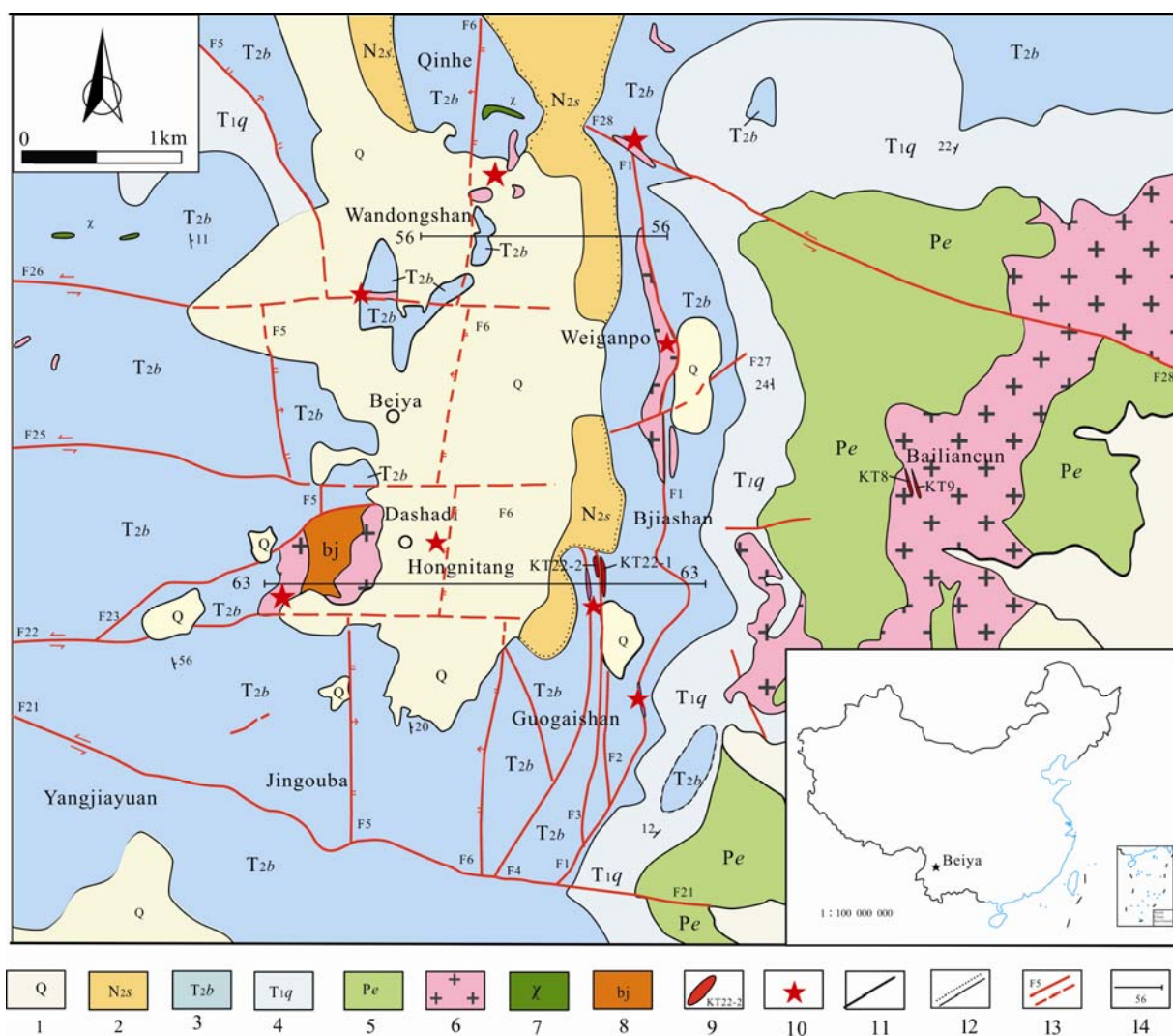


Fig. 1. A simplified Geological map of the Beiya gold-polymetallic deposit (China basemap after China National Bureau of Surveying and Mapping Geographical Information)

(1), Quaternary elurium; (2), Pliocene Sanying Formation, sandy conglomerate and claystone; (3), Middle Triassic Beiya Formation, argillaceous limestone and dolomite; (4), Lower Triassic Qingianbao Formation, sandy conglomerate and sandstone; (5), Upper Permian Emeishan basalt Formation, basalt intercalating tuff; (6), quartz syenite porphyry; (7), lamporphyer vein; (8), cryptoexplosive Breccia; (9), ore-bodies and their serial numbers; (10), site of rock body; (11), geological boundary; (12), uncomformable boundary; (13), measured and inferred faults as well as their serial numbers; (14), exploration lines and their serial numbers.

stratiform in the contact zone; 3) an Fe–Au–Pb–Ag or Fe–Cu ore body occurring as stratoid and large lenticular shapes, hosted in the interlayer fracture zone of the  $T_{2b}$  carbonate rocks near the contact zone; and 4) a Pb–Zn–Ag ore body occurring as small lenticulars and veins, in the fracture and fissure zone of the  $T_{2b}$  carbonate rocks apart from the contact zone. More than 1,800 polymetallic ore bodies exist in the ore district, composed of Au, Fe, Cu, Ag, Pb, and Zn, which includes more than 50 relatively large ore bodies. The main ore bodies are KT4, KT10, KT11, KT52, KT54, as well as KT63, and the amount of gold within a single ore body classifies each as greater than a medium-sized deposit (YGMGC, 2014). The main ore body is 400–1,680 m long and 570–1,420 m wide, with an average thickness of 4.27–13.27 m and an average

grade of 1.65–2.83ppm Au, 25.06–37.55% TFe, 18.47–28.11% mFe, 0.63–0.65% Cu, 0.91–4.04% Pb, 0.28–1% Zn, as well as 24.52–67.29ppm Ag. The main characteristics of a typical ore body are illustrated in Table 1 and Figure 2. The weathering-accumulation type ore bodies are hosted in  $N_{2s}$ , with a length of 1,840 m along the strike, a width of 0.90–35.32 m and a grade of 0.90–20.24ppm Au, 25.06–63.63% TFe, 0.10–1.29% Cu, 1.21–2.04% Pb, 0.23–0.70% Zn, as well as 15.36–23.33ppm Ag.

Primary ores are composed of a number of metallic minerals, such as magnetite, pyrite, chalcopyrite, siderite, hematite, galena, pyrrhotite, and sphalerite. Oxidized ores contain mainly limonite, malachite, galena, cerussite, smithsonite, and cerargyrite. Gangue minerals include

Table 1 Geological features of main ore bodies within the Beiya gold-polymetallic deposit

Deposit type	Skam type in the contact zone of the Wangdongshan porphyry body	Skam type in the contact zone of the Hongnitang porphyry body	Skam type in the contact zone of Dashadi porphyry body	Residual type
Main mineralized elements	Au-Fe-Cu (Mo)	Au-Fe-Cu, Cu-Fe, Pb-Ag	Cu-Fe	Au-Fe
Typical ore body	KT52 ore body	KT10 ore body	KT18 ore body	KT4B ore body
Characteristics of ore body	<p>The ore body in the Wangdongshan ore section occurs in the exocontact zone between alkali-rich porphyry and <math>T_{2b}</math> carbonate rocks as stratiform, showing ring distribution around rock body, and its occurrence varies synchronously with the contact zone of the rock body, with a length of 1,680 m in SN (strike) direction, a width of 113–1,420 m in the EW direction and a thickness of 0.8–115.26 m. Au: 0.86–239 ppm; TFe: 22.37–66.94%; mFe: 16.04–52.46%; Cu: 0.20–25.72%; Pb: 0.40–1.12%; Zn: 0.13–0.45%; Ag: 29.75–44.60 ppm. Identified resource reserves: Au &gt; 200t, Cu &gt; <math>3 \times 10^5</math> t, total iron ore &gt; <math>1.1 \times 10^8</math> t, Ag &gt; 4000 t</p>	<p>The ore body in the Hongnitang ore section occurs in skarn of the contact zone between the Hongnitang porphyry and <math>T_{2b}</math> carbonate rocks as lenticular-stratiform. The length is 1,600 and 174–540 m along the strike, a width of 100–810 m and a thickness of 0.81–24.49 m, with an average value of 5.51 m of the ore body. Au: 0.81–19.30 ppm, ave. of 2.48 ppm; mFe: 25.03–49.36%, ave. 32.73%; Pb: 1.02–16.42%, ave. 2.71%; Zn: 1.31–4.51%, ave. of 1.86%; Ag: 1.90–842.7 ppm, ave. of 86.76 ppm. Identified resource reserves: Au &gt; 10 t, Cu &gt; <math>2 \times 10^4</math> t, total iron ore &gt; <math>6 \times 10^6</math> t, Ag &gt; 360 t</p>	<p>The ore body in the Hongnitang ore section occurs in skarn of the contact zone between the Dashadi porphyry and <math>T_{2b}</math> carbonate rocks as lenticular-stratiform, dips to W direction steeply. The length is 640 m along the strike, the extension depth is from 115 m to 385 m, and the thickness is between 1.12 m and 32.5 ppm; mFe: 25.03–49.36%, ave. 32.73%; Pb: 1.21–2.04%; Zn: 0.23–0.70%; Ag: 15.36–23.33 ppm. Identified resource reserves: Au &gt; <math>8 \times 10^4</math> t, Cu = <math>7 \times 10^4</math> t, iron(TFe) &gt; <math>4 \times 10^6</math> t, Ag = 80 t</p>	<p>The ore body in the Wangdongshan -Hongnitang ore section occurs in unconformable contact surface between <math>T_{2b}</math> and <math>N_{2s}</math> as stratiform. The length is 1,840 m along the strike, the width is from 420 m to 500 m, and the thickness is between 0.90 m and 35.32 m. Au: 0.90–20.24 ppm; TFe: 25.06–63.63%; Cu: 0.10–1.29%; Pb: 1.21–2.04%; Zn: 0.23–0.70%; Ag: 15.36–23.33 ppm. Identified resource reserves: Au &gt; <math>8 \times 10^4</math> t, Cu = <math>7 \times 10^4</math> t, iron(TFe) &gt; <math>4 \times 10^6</math> t, Ag = 80 t</p>
Metallic minerals	Magnetite, pyrrhotite, pyrite, chalcopyrite, siderite, hematite, limonite, and cerussite	Magnetite, pyrrhotite, siderite, hematite, pyrite, chalcopyrite, and galena	Magnetite, hematite, pyrite, chalcopyrite, molybdenite, and galena	Limonite, cerussite, and magnetite
Gangue minerals	Garnet, diopside, chlorite, epidote, calcite, dolomite and quartz	Calcite, dolomite, quartz, feldspar, garnet and epidote	Quartz, feldspar, diopside, chlorite, epidote and kaolin	Clay and gravel
Ore texture and structure	Poikilitic, xenomorphic granular, euhedral, metasomatic relict, massive and star point structures, etc.; the oxide ores occur as pseudomorphic, colloform, honeycomb, earthy, and powder structures, etc.	Xenomorphic granular, metasomatic relict, honeycomb, earthy, and powder structures, etc.	Granular, poikilitic, metasomatic relict, massive, star point structures, etc.	Colloform, pseudomorphic, honeycomb, earthy, powder and massive structures
Alteration type	Skarnization, silicification, marblization, carbonatization, magnetitization, pyritization, chalcocopyritization, and molybdenitization	Silicification, carbonatization, magnetitization, pyritization, chalcocopyritization, galenitization, and sphaleritization	Silicification, skarnization, magnetitization, pyritization, chalcocopyritization, and molybdenitization	Limonitization and calcitization
Ore-controlling factors	The ore controlled by the contact alteration zone of the Wangdongshan rock body in branches and bifurcate of the rock body, protruding and turning parts	Interlayer fracture zone, secondary fault and fissure zone, prostrated zone	Ore controlled by contact alteration zone of the Hongnitang rock body with a steep, gentle occurrence change of the rock body and the transition position	Unconformable contact surface
Scale of ore body	All Cu deposits in superlarge scale, and co-associated deposits of Pb, Zn, Ag, Cu and Fe in medium to large scale.	Au deposits in medium-large scale, and the co-associated deposits of Fe, Pb-Zn and Ag in small to medium scale.	Au deposits in medium scale, and the co-associated deposits of Pb-Zn and Ag in the small-to-medium scale.	Au deposits in the small-to-medium scale, and the co-associated deposits of Fe and Ag in small-medium scale.
Ore bodies of the same type	Branch ore bodies of KT52, etc.	KT43, KT46, KT49 (interior of rock body), KT6, KT13, KT15, KT22, KT20, KT31–32, KT54–57, etc.	KT11 and KT12	KT1, KT3, KT4A–KT4E, KT5, etc.

**Table 2 Major (wt%), trace (ppm) and rare earth (ppm) element results for the ore-forming rock bodies related to the Beiya Au-polymetallic deposit**

Chemical composition	Wangdongshan rock body (quartz syenite porphyry)			Hongnitang rock body (quartz syenite porphyry)			Dashadi rock body (quartz monzonite porphyry)		
	Min.	Max.	Mean (pieces)	Min.	Max.	Mean (pieces)	Min.	Max.	Mean (pieces)
SiO <sub>2</sub>	69.42	72.82	70.67(5)	67.79	71.44	69.92(8)	65.31	69.86	67.95(8)
TiO <sub>2</sub>	0.15	0.24	0.19(5)	0.19	0.87	0.32(8)	0.17	0.17	0.17(2)
Al <sub>2</sub> O <sub>3</sub>	13.45	15.26	14.51(5)	14.76	16.03	15.21(8)	17.43	17.64	17.54(2)
Fe <sub>2</sub> O <sub>3</sub>	0.55	2.09	1.38(5)	0.20	2.12	0.93(8)	1.19	1.47	1.33(2)
MnO	0.01	0.08	0.03(5)	0.01	0.28	0.08(8)	0.02	0.02	0.02(2)
MgO	0.11	0.32	0.23(5)	0.04	0.35	0.15(8)	0.56	0.57	0.56(2)
CaO	0.21	1.06	0.49(5)	0.02	0.34	0.17(8)	1.05	1.06	1.05(2)
Na <sub>2</sub> O	1.15	4.09	2.62(5)	0.38	2.66	1.23(8)	3.39	4.93	4.16(2)
K <sub>2</sub> O	6.16	9.09	7.36(5)	8.50	12.15	10.41(8)	5.57	6.93	6.25(2)
P <sub>2</sub> O <sub>5</sub>	0.07	0.12	0.09(5)	0.02	0.16	0.06(8)	0.11	0.12	0.11(2)
LOI	1.29	1.79	1.53(5)	0.52	1.65	1.01(8)	1.33	1.35	1.34(2)
TOTAL	97.55	100.5	99.12(5)	98.61	99.83	99.43(8)	99.63	99.72	99.68(2)
K <sub>2</sub> O + Na <sub>2</sub> O	9.30	10.25	9.99(5)	10.75	12.53	11.649(8)	10.32	10.50	10.41(2)
K <sub>2</sub> O/Na <sub>2</sub> O	1.51	7.90	3.53(5)	3.48	31.97	14.41(8)	1.13	2.04	1.59(2)
A/CNK	0.99	1.25	1.11(5)	0.98	1.27	1.13(8)	1.10	1.16	1.13(2)
Rb	177	262	201.2(5)	169	502	428.87(8)	196.88	243.37	220.13(2)
Ba	1894	3437	2389(5)	2008	2784	2380(8)	2240.4	2251.4	2245.9(2)
Th	10.07	13.86	11.57(5)	7.72	14.20	11.87(8)	13.73	15.17	14.45(2)
U	2.79	10.24	5.27(5)	2.89	7.03	4.31(8)	2.98	3.59	3.29(2)
Nb	8.69	11.75	9.62(5)	8.10	10.59	9.34(8)	10.02	10.99	10.60(2)
Ta	0.60	0.85	0.75(5)	0.51	1.09	0.73(8)	0.62	0.65	0.63(2)
La	5.81	19.50	13.10(5)	16.24	28.40	23.09(8)	17.88	26.36	22.09(2)
Ce	14.80	34.20	25.45(5)	27.82	54.80	43.72(8)	37.19	46.51	41.85(2)
Pb	15.60	51.86	28.02(5)	43.44	756.13	320.83(8)	26.94	28.57	27.76(2)
Sr	365	788	584.8(5)	320	1240	572(8)	843.34	981.98	912.66(2)
Nd	7.01	12.80	10.45	9.82	24.0	15.61(8)	16.36	16.59	16.48(2)
Zr	141	171	153.6(5)	139	198	166.87(8)	53.80	68.07	60.94(2)
Hf	4.28	4.96	4.52(5)	4.39	5.94	5.01(8)	2.49	2.79	2.64(2)
Sm	1.56	2.46	2.06(5)	1.77	6.20	3.12(8)	3.77	3.79	3.78(2)
Gd	1.41	2.11	1.81(5)	1.63	5.60	2.72(8)	2.70	2.80	2.75(2)
Ho	0.24	0.30	0.27(5)	0.24	0.88	0.40(8)	0.32	0.34	0.33(2)
Y	6.45	8.50	7.50(5)	2.70	9.43	6.78(8)	9.42	10.24	9.83(2)
Yb	0.62	0.81	0.72(5)	0.63	1.80	0.96(8)	0.79	0.86	0.83(2)
Lu	0.09	0.12	0.11(5)	0.10	0.25	0.13(8)	0.12	0.13	0.12(2)
Pr	1.57	3.62	2.73(5)	2.82	7.60	4.65(8)	4.58	5.01	4.82(2)
Sm	1.56	2.46	2.06(5)	1.77	6.20	3.12(8)	3.77	3.79	3.78(2)
Eu	0.30	0.72	0.51(5)	0.33	1.80	0.99(8)	1.17	1.20	1.19(2)
Gd	1.41	2.11	1.81(5)	1.63	5.60	2.72(8)	2.70	2.80	2.75(2)
Tb	0.21	0.29	0.25(5)	0.21	0.76	0.35(8)	0.34	0.36	0.35(2)
Dy	1.18	1.55	1.41(5)	1.19	4.20	1.99(8)	1.71	1.86	1.76
Er	0.62	0.81	0.71	0.65	2.20	1.06(8)	0.88	0.94	0.91
Tm	0.10	0.12	0.11(5)	0.10	0.33	0.15(8)	0.12	0.13	0.13

Note: The data listed in the table are statistics based on the analytical results of a single sample. Samples were analyzed in the Key Laboratory of Orogenic Belts and Crustal Evolution, Peking University. Major elements were determined by X-ray fluorescence (XRF). The instrument used is ARLADVANTXP+ (Thermo Electron Company of the United States), and the precision is better than 1%. Trace elements and REE were analyzed by inductively coupled plasma mass spectrometry (ICP-MS), using Agilent ICPMS7500ce mode instrument (American Agilent Technologies). The analytical precision is higher than 5%.

quartz, calcite, garnet, diopside, wollastonite, scapolite, chlorite, epidote, dolomite, and kaolinite. The primary ores have poikilitic, xenomorphic granular, euhedral, as well as metasomatic relict textures, with massive and disseminated structures. Oxidized ores have pseudomorphic, colloform, honeycomb, earthy, and powder structures.

## 2.3 Metallogenic geological characteristics of the deposit

### 2.3.1 Distribution characteristics of alkali-rich porphyry intrusions

There are eight Himalayan alkali-rich porphyries exposed throughout the ore district (Fig. 1), located near the core of the Beiya syncline, where the distribution is

mainly controlled by the four sets of faults. In addition to the buried Dashadi rock body, there are seven other rock bodies exposed at the surface, with a total area of 0.34 km<sup>2</sup>. The semi-buried Wangdongshan rock body, the buried Dashadi rock body, and the semi-buried Hongnitang rock body are the main metallogenic rock bodies, of a relatively large scale, and occur as a stock, whereas the remaining ones occur as veins, dikes, and sills.

The semi-buried Wangdongshan stock is distributed throughout the Wangdongshan ore section in the northern part of the ore district, with a nearly SN strike, generally dipping to the west, decreasing in elevation from north to south, and pitching to the southwestern side. The length in the SN direction is 1,300 m, the width in the EW direction is between 100 and 500 m, and the extended depth

between exploration lines 60 and 80 is between 500 and 600 m (not a closed boundary). The rock body is exposed intermittently on the surface, between exploration lines 68 and 96, has a length of 470 m in the SN direction, and a width between 30 and 65 m in the EW direction. Between exploration lines 48 and 100, the rock body extends in depth below 1,700 m in elevation, with a length of 1,100 m in the SN direction and a width of 600 m in the EW direction. Between exploration lines 56 and 72, the maximum width of the rock body is approximately 600 m, and the lowest controlled elevation is 1,352 m. The hanging wall contains more regular occurrences of the contact zone, whereas the presence of the contact zone is more complex in the footwall, with a general dip angle of 43–85° (Fig. 2a). Well-developed rock body structures at the contact zone contain the majority of the skarn zone and the main ore body deposits. Steep, hydrothermal, vein-shaped ore bodies occur along well-developed fissures in

the rock body interior.

The semi-buried Hongnitang rock body appears in regions with steep slopes in the western margin of the basin, in the west side of the Hongnitang ore section and the southern part of the ore district. It is exposed between exploration lines 43 and 71, with a length of 480 m in the SN direction and a width of approximately 160–190 m in the EW direction. Shattered and crypto-explosive breccia exists on the eastern surface. The exposed surface elevation is between 2,100 and 1,950 m, and the depth is controlled by drill holes along exploration line 55, with a minimum controlled elevation of 1,378 m. The rock body (stock) strikes toward the SN and dips westward with a gentle dip angle of less than 10° above 1,900 m and a relatively steep dip angle of 20–30° below 1,900 m. The hanging wall has a contact with the fourth section of the Beiya formation, and there is a constant contact zone occurrence, with a dip angle between 10° and 20°. The

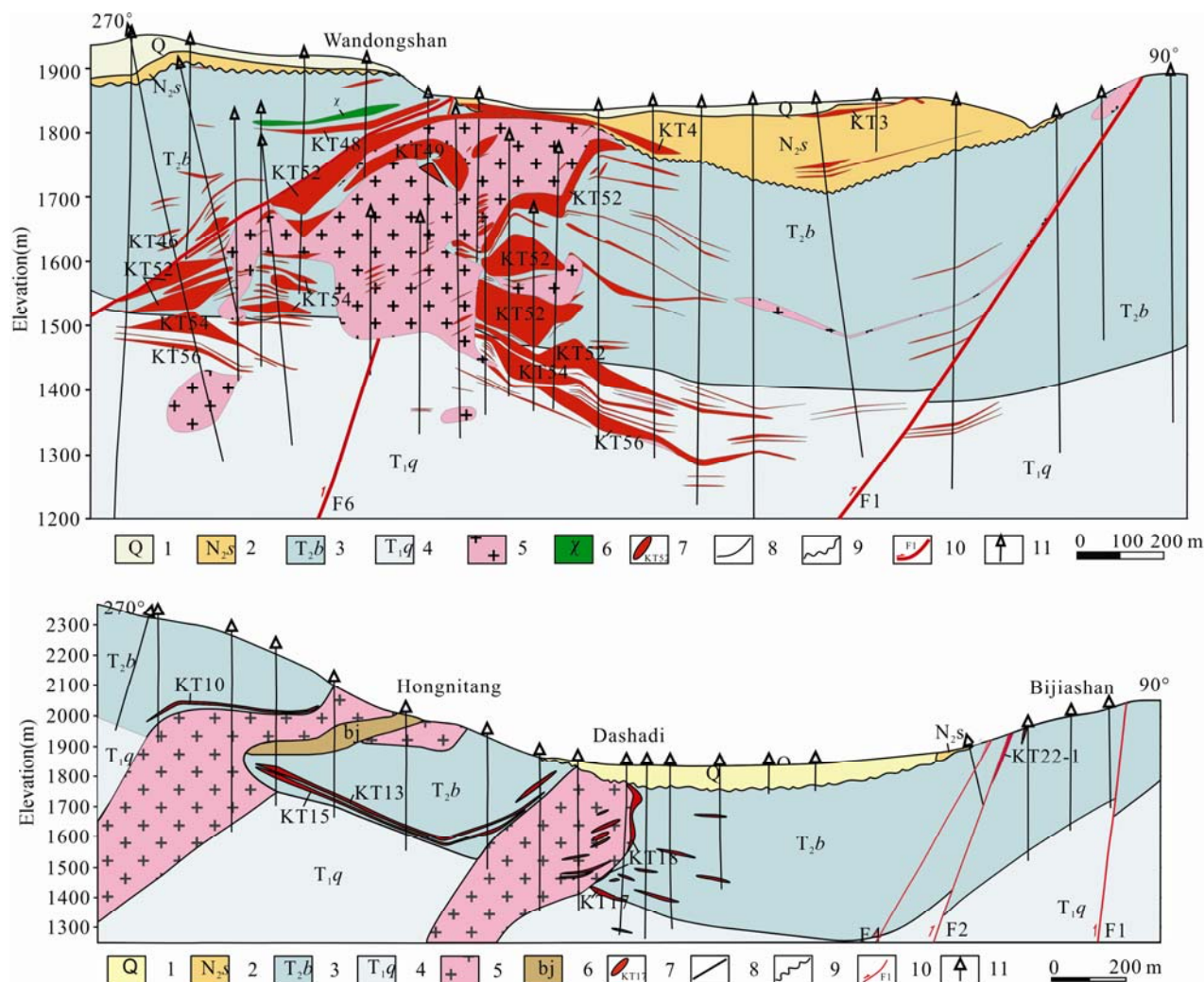


Fig. 2. Geological section along No. 56 and No. 63 exploration lines in the Beiya gold-polymetallic deposit.

(1), Quaternary elurium; (2), Pliocene Sanying Formation, sandy conglomerate and sand-gravel-bearing claystone; (3), Middle Triassic Beiya Formation, carbonete rock; (4), Lower Triassic Qingianbao Formation, sandstone; (5), quartz syenite porphyry; (6), lamporphyer vein; (7), ore-bodies and their serial numbers; (8), geological boundary; (9), uncomformable boundary; (10), measured and inferred faults as well as their serial numbers; (11), drill hole.

occurrence of the contact zone in the footwall is more complex, with an overall dip angle of 35–40°. Well-developed rock body structures at the contact zone contain the majority of the skarn zone and the main ore body deposits (Fig. 2b).

The buried Dashadi rock body is located in the central zone of the Beiya basin, between exploration lines 47 and 71 in the middle of the Hongnitang ore section, in the southern part of the ore district. It is to the east side of the Hongnitang rock body, where the horizontal distance between the two is generally 400–700 m, with a slightly lower elevation than that of the Hongnitang rock body (42–300 m lower). The rock body occurs in the form of a stock (spindle), with a southward pitch, dipping to the west at an angle of 40–88°, and has an extended depth from 240–320 m along its dip. The length along the SN strike is 720 m; the width along the EW dip is 100–750 m; and the distribution height is between 1,818 and 1,220 m (Fig. 2b). The contact interface between the Dashadi rock body and the Beiya wall rock is irregularly concave and convex. There are well-developed skarn zones in both the east and west contact zones of the rock body, mainly Fe and Cu (Mo) deposits (mineralization). At the edge of the rock body, there are areas of chloritization and partial silicification, accompanied by limonitization, pyritization, chalcopyritization, molybdenitization, lead and zinc mineralization, as well as magnetitization. The interior of the rock body is strongly altered by pyritization, chalcopyritization, and molybdenitization.

In the eastern part of the ore district, the Bijiashan and Weiganpo dyke occur intermittently along the F<sub>1</sub>, F<sub>2</sub>, and F<sub>3</sub> faults, with lengths of 460, 400, and 1,700 m as well as widths of 5–11, 3–13, and 50–120 m, respectively. They strike in the SN direction and dip westward at a dip angle of 20–40°, 60–78°, and 30–40°, respectively. Vein-shaped as well as lenticular Fe–Au and Pb–Ag mineralization is present in veins in the contact zone near the F<sub>2</sub> and F<sub>3</sub> faults and at the interlaminar fracture zone.

In the ore district, the lamprophyre and late biotite syenite porphyry veins are common along secondary faults and cut the quartz syenite porphyry and ore bodies. They formed later, with little to no association with mineralization.

### 2.3.2 Petrological characteristics of the alkali-rich porphyry intrusive body

The lithologies of the Wandongshan and Hongnitang rock bodies are quartz syenite porphyry, with a gray–white color, whose surface has been altered by limonitization, with some instances of chloritization. These rocks have a porphyritic texture and contain phenocrysts of orthoclase and quartz (50–60%). The orthoclase phenocrysts have

euhedral–subhedral tabular textures (35–45%). Carlsbad twinning is visible with a hexagonal shape, and granularity of 0.5–4.0 mm. Occasionally, crystals exhibit alteration patterns that formed metasomatic relict textures (Fig. 3a and b). The surface of the quartz is clean, and the grain size is between 0.1 and 3.0 mm (5–10%). The crystals are irregular, mostly with a round and embayed shape, because of corrosion. Plagioclase phenocrysts occasionally occur as short column subhedrons, with obvious polysynthetic twinning, which is often replaced and intercalated with late-stage potassium feldspar. The matrix is cryptocrystalline and composed of feldspar as well as quartz. Accessory minerals include apatite, zircon, and titanite. Mineralization of magnetite, pyrite, galena, sphalerite, and chalcopyrite has been identified locally. The quartz syenite porphyry is strongly altered by potassium. Plagioclase crystals, in which sericitization is common, have potassium feldspar free rims. Quartz phenocrysts have dissolved into an embayed shape, and the matrix has also been altered. Additionally, fresh potassium feldspar phenocrysts are visible.

The Dashadi rock body contains quartz monzonite porphyry, with a gray-off–white color, a porphyritic texture, and a massive structure. Phenocrysts are mainly potash feldspar (40%), with a subhedral shape, and particle sizes ranging from 2 to 6 mm. Carlsbad twinning, as well as potash feldspar sericitization, is visible under cross-polarized light (Fig. 3c). Plagioclase (25%) is hypautomorphic, with a particle size of 2–4 mm. Polysynthetic twinning and plagioclase sericitization are both visible under microscope. Quartz (25%) occurs as xenomorphic grains, with a grain diameter of approximately 3 mm. Matrix components are predominantly quartz and feldspar, as well as accessory minerals, such as zircon and sphene, with minor amounts of pyrite.

Lithologies in the Bijiashan and Weiganpo bodies, in the eastern region, are all quartz monzonite porphyry, with a grayish brown color, a porphyritic texture, and a massive structure. The phenocrysts are orthoclase and plagioclase (Fig. 3d–f), with contents between 50% and 65%. Orthoclase (30–40%) has a euhedral–subhedral texture, mostly altered to relict textures, and the crystal grain size is between 2 and 5 mm. Plagioclase (15–20%) is transparent, white, and subhedral. Quartz (<5%) contains minor amounts of biotite, plagioclase, and hornblende. The matrix (30–40%) is mainly composed of plagioclase and potash feldspar, with signs of weak sericitization.

## 3 Method and Results

### 3.1 Geochemical analysis of alkali-rich porphyry

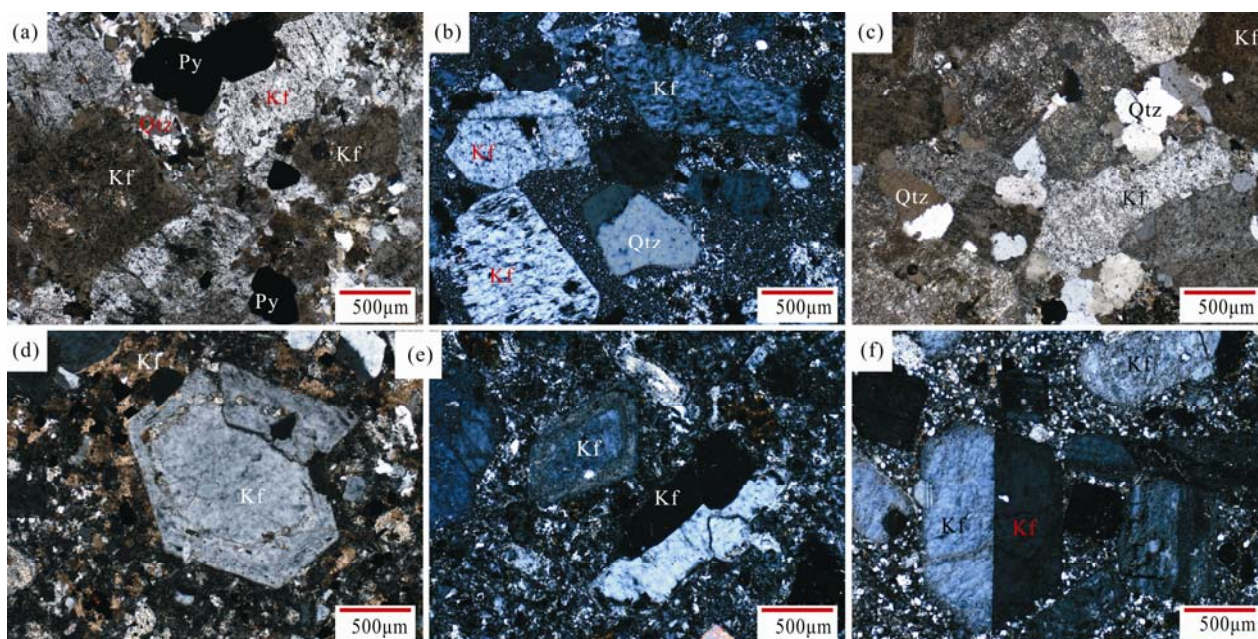


Fig. 3. Microscopic characteristics of the porphyries in the Beiya ore district.

(a), potash feldspar phenocryst, dissolution into an embayed shape at the edge of the quartz phenocryst, with pyritization in the Wandongshan quartz syenite porphyry; (b), potash feldspar phenocryst, dissolution into an embayed shape at the edge of the quartz phenocryst in the Hongnitang quartz syenite porphyry; (c), potash feldspar phenocryst with sericitization, dissolution into an embayed shape at the edge of the quartz phenocryst in the Dashadi quartz monzonite porphyry; (d), albite ring formed by Na-replacement at the edge of the potash feldspar in the quartz monzonite porphyry, with sericitization; (e), albite ring formed by Na-replacement at the edge of the potash feldspar in the quartz monzonite porphyry, with plagioclase polysynthetic twins and biotite phenocrysts; (f), plagioclase polysynthetic twins in the quartz monzonite porphyry; Qtz - quartz, Kf - potash feldspar, Py - pyrite, Bt - biotite, Pl - plagioclase.

### intrusive body

Fresh samples were collected from the semi-buried Wandongshan, the buried Dashadi, and the semi-buried Hongnitang rock bodies from drill cores and open mining pits. The major, trace, and rare earth elements were analyzed at the Key Laboratory of Orogenic Belts and Crustal Evolution, Peking University. Geochemical results are presented in Table 2.

#### (1) Major elemental characteristics

The quartz syenite and quartz monzonite porphyries, in the ore district, were classified as acidic rocks (the content of  $\text{SiO}_2$  is between 65.31% and 72.82%) with a relatively high total alkali content (the content of  $\text{K}_2\text{O} + \text{Na}_2\text{O}$  is between 9.30% and 12.53%). On a TAS diagram, most samples were plotted in the quartz monzonite and alkaline series field (Fig. 4a). On a  $\text{SiO}_2$ - $\text{K}_2\text{O}$  diagram, samples were plotted in the shoshonite series field (Fig. 4b). The  $A/\text{CNK}$  values ( $\text{Al}_2\text{O}_3/(\text{CaO}+\text{K}_2\text{O}+\text{Na}_2\text{O})$  mole ratio) are between 0.91 and 1.65, which belong to the metaluminous-peraluminous series (Fig. 4c). The  $\text{Al}_2\text{O}_3$  and  $\text{Na}_2\text{O}$  contents of most samples decrease with increasing  $\text{SiO}_2$  content. Compared with the quartz monzonite porphyry, the quartz syenite porphyry is more acidic ( $\text{SiO}_2$  content of 67.79–72.82%), with a higher  $\text{K}_2\text{O}$  content (6.16–12.15%) and  $\text{K}_2\text{O}/\text{Na}_2\text{O}$  ratio (1.51–31.97) as well as decreased  $\text{Al}_2\text{O}_3$  (13.45–16.03%),  $\text{CaO}$  (0.45–1.06%), and  $\text{Na}_2\text{O}$  (0.38–4.09%) contents. The  $\text{TiO}_2$  varies between the

different quartz monzonite porphyries (0.15–0.87%). Due to strong potassic alteration, the quartz syenite porphyry, at Hongnitang, has a higher  $\text{K}_2\text{O}$  content (8.50–12.15%) and  $\text{K}_2\text{O}/\text{Na}_2\text{O}$  ratio (3.48–31.97) as well as decreased  $\text{CaO}$  (0.02–0.34%) and  $\text{Na}_2\text{O}$  (0.38–2.66%) contents compared with the quartz syenite porphyry at Wandongshan.

#### (2) Trace elemental characteristics

The primitive mantle-normalized diagram (Fig. 5a) indicates that the trace element distribution curve is inclined to the right. The quartz syenite and quartz monzonite porphyry have similar trace elemental compositions, i.e. they are rich in the large ion lithophile element (LILE; e.g., Rb, K, Sr, and Pb) and are depleted in the high field strength elements (HFSE; e.g., Ta, Nb, P, Ti, and HREE); this is evidence of comagmatic evolution. Compared with the quartz monzonite porphyry, the quartz syenite porphyry has increased Rb (168–538 ppm), Ba (1,160–5,547 ppm), and Pb (15.60–756.13 ppm) contents as well as decreased Nb (7.01–24 ppm), La (5.81–28.4 ppm), Ce (14.8–54.8 ppm), and Y (2.7–12.25 ppm) contents. The quartz syenite porphyry, at Hongnitang, relative to other rock bodies, has the highest Rb, Ce, La, and Pb contents.

#### (3) Rare earth element characteristics

The chondrite-normalized spidergram (Fig. 5b) indicates that the rare earth element (REE) distribution

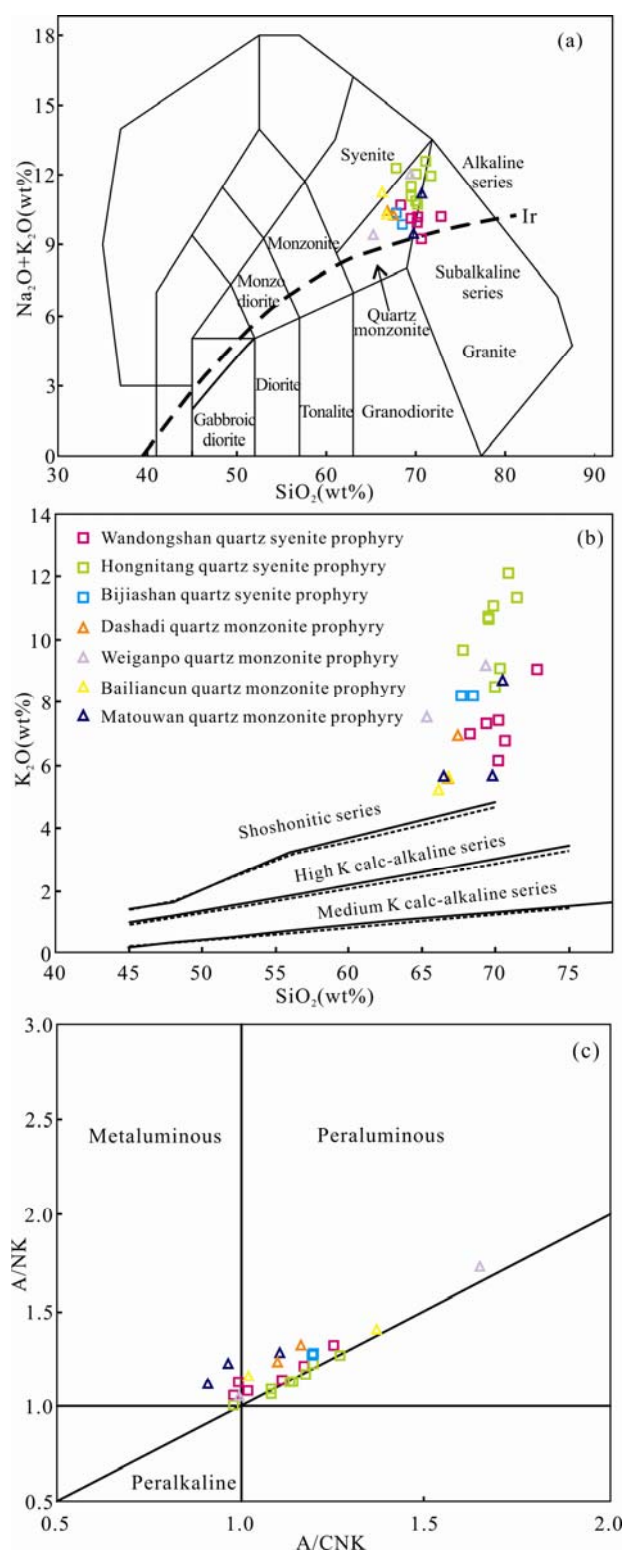


Fig. 4. Classification diagrams for the geochemistry of the ore-forming porphyries in the Beiya ore district.

(a), TAS diagram (after Middlemost, 1994 as well as Irvine and Baragar, 1971); (b),  $\text{K}_2\text{O}$  vs.  $\text{SiO}_2$  diagram (after Peccerillo and Taylor, 1976 as well as Middlemost, 1985); (c), A/NK vs. A/CNK diagram (after Chapal and White, 1974 as well as Maniar and Piccoli, 1989).

curve is inclined to the right. The quartz syenite and quartz monzonite porphyry have similar REE distribution

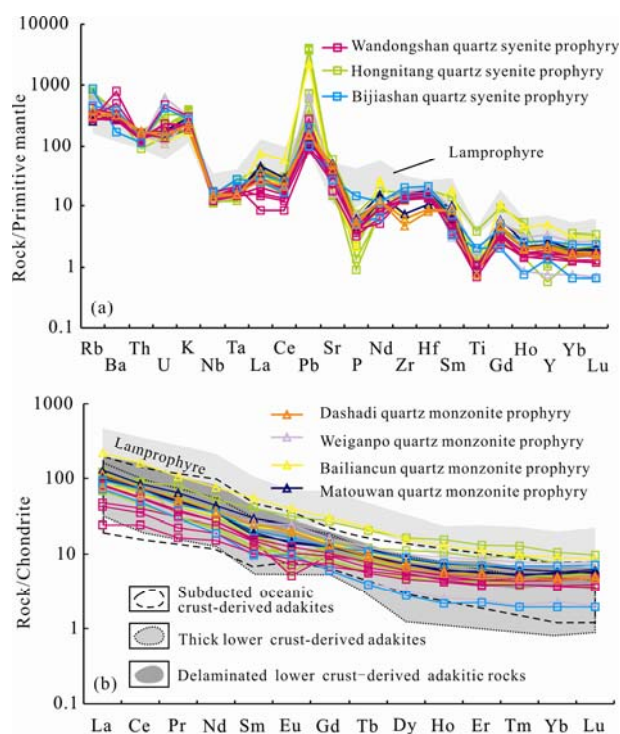


Fig. 5. A primitive mantle-normalized trace element spider diagram (a) and chondrite-normalized REE patterns (b) for the ore-forming porphyries in the Beiya Au-polymetallic deposit.

Data source: Normalized values of primitive mantle and chondrites (after Sun and McDonough, 1989).

patterns, which display relatively low total REE contents (SREE=36.3–503.6 ppm, with an average value of 138.53 ppm), light rare earth element enrichments (LREE), and a depletion of the heavy rare earth elements (HREE; LREE/HREE=7.06–14.26). The  $(\text{La}/\text{Yb})_N$  ratio varies between 5.15 and 39.43. The REE compositions of most samples have weak to moderate negative Eu anomalies ( $\text{Eu}=0.42\text{--}0.99$ ), but the quartz monzonite porphyry, at Dashadi, does not display any obvious negative Eu anomaly. The quartz syenite porphyry has a higher total REE content and  $(\text{La}/\text{Yb})_N$  ratio as well as a weaker negative Eu anomaly compared with the quartz monzonite porphyry. Additionally, the total REE content in the Wandongshan quartz syenite porphyry is relatively low.

### 3.2 Intrusion ages of the alkali-rich porphyries

Three quartz syenite and quartz monzonite porphyry samples from the Wandongshan, Hongnitang, and Dashadi rock bodies related to the Beiya deposit were analyzed by LA-MC-ICP-MS zircon U–Pb geochronology at the Institute of Mineral Resources, Chinese Academy of Geological Sciences. The analytical results indicate that the rock-forming ages of the semi-buried Wandongshan, the buried Dashadi, and the semi-buried Hongnitang rock bodies are  $35.00 \pm 0.17$  Ma,  $35.06 \pm 0.16$  Ma, and

36.72±0.25 Ma, respectively. Combined with previous geochronological studies, the quartz syenite and quartz monzonite porphyry (Table 3) intruded between 34.62 and 36.72 Ma, with a younger emplacement age of 35.56 Ma for the biotite quartz syenite porphyry. These ages agree with the formation ages of the alkali-rich porphyries throughout the region (Yan et al., 2017; Cui et al., 2017; Zhu et al., 2013).

## 4 Discussion

### 4.1 Alkali-rich porphyry

#### 4.1.1 Source and genesis of the alkali-rich porphyries

In the ore district, the quartz syenite porphyry, compared with the quartz monzonite porphyry, has higher contents of SiO<sub>2</sub>, K<sub>2</sub>O, Rb, Ba, and Pb, larger K<sub>2</sub>O/Na<sub>2</sub>O ratios, as well as lower contents of Al<sub>2</sub>O<sub>3</sub>, CaO, Na<sub>2</sub>O, Nb, La, and Ce, which are possible due to the insignificant amount of plagioclase and the presence of strong, potassic alteration in the quartz syenite porphyry. The high Fe<sub>2</sub>O<sub>3</sub> content, in the quartz syenite, is possibly a result of limonitization, and the high MgO content may derive from the large amount of hornblende. Although there are some differences between the quartz syenite and quartz monzonite porphyry, they have similar textures, SiO<sub>2</sub> content, trace element compositions and REE distribution patterns, indicating that they have similar sources.

The porphyries in the ore district have a relatively elevated Sr content and Sr/Y ratio, a decreased amount of Y and Yb, enrichment in the LILEs, and depletions in the HFSEs, which are similar to the characteristics of the adakitic rocks formed by the partial melting of a subducting slab (Richards and Kerrich, 2007; Jia Tuya et al., 2016). However, the porphyries differ from the adakitic rocks because they have a higher K<sub>2</sub>O content and

lower MgO, Cr, and Ni contents, indicating that the alkaline rock bodies of the Beiya ore district and adakitic rocks both formed by partial melting of a subducting slab but from different source areas in different geodynamic settings.

The rock bodies have a high K<sub>2</sub>O content, which may be caused by a potassium-enriched source and/or the upper crust. Electron probe results indicate that potash feldspars have high K<sub>2</sub>O/Na<sub>2</sub>O ratios and that the potash feldspar formed by potassic alteration has a higher K<sub>2</sub>O content and K<sub>2</sub>O/Na<sub>2</sub>O ratios than those formed by fractional crystallization. The developed melts and fluids are both rich in K, suggesting that the magma source is also rich in K. Additionally, zircons have high δO<sup>18</sup> values (Lu et al., 2013), and the rock body contains dark microgranular enclaves. The higher K<sub>2</sub>O content may be related to an upper crustal mixture. However, Hf isotopic results for zircon ( $\epsilon_{\text{Hf}}(t) = -6.82-4.9$ ) indicate that mixing of the upper crust is limited. Only crustal contamination can cause such a high K<sub>2</sub>O content (higher than the upper crustal average). Therefore, this suggests that the high K<sub>2</sub>O content of the rock body originates from a combination of a high K source area and a certain degree of upper crustal material mixture.

The rock bodies have a higher SiO<sub>2</sub> content and (La/Yb)<sub>N</sub> ratios as well as lower MgO, Cr, Ni, Co, and V contents, indicating that they formed by partial melting of the crust rather than that of the mantle (Wyllie, 1977). Weak–very weak negative Eu anomalies imply that the rock bodies formed in the thickened lower crust (Deng Wanming et al., 1998). Hf isotopic zircon values vary widely, thus indicating the diversity of zircon sources. Positive  $\epsilon_{\text{Hf}}(t)$  values reflect zircons that formed in the juvenile lower crust, whereas negative  $\epsilon_{\text{Hf}}(t)$  values indicate that zircons formed in the ancient metamorphic basement (Lai et al.,

**Table 3 Geochronological data for the main ore-forming rock bodies in the Beiya Au–polymetallic deposit**

Rock body	Rock type	Testing mineral	Testing method	Age (Ma)	Reference
Wangdongshan rock body	Monzogranite porphyry	Zircon	LA-MC-ICP-MS U-Pb	36.34–36.79	He 2014
	Biotite monzogranite porphyry	Zircon	LA-MC-ICP-MS U-Pb	35.56±0.20	He 2014
	Quartz syenite porphyry	Zircon	SHRIMP U-Pb	33.3±1.50	Xu et al., 2007
	Altered quartz syenite porphyry	Muscovite	Ar-Ar	32.5±0.09	Ying et al., 2004
	Quartz syenite porphyry	K-feldspar	Ar-Ar	25.53±0.25	Ying et al., 2004
	Quartz syenite porphyry	Zircon	LA-MC-ICP-MS U-Pb	36.07±0.43	Fu et al., 2015
	Porphyritic granite	Zircon	LA-MC-ICP-MS U-Pb	34.95–37.03	Deng et al., 2015
	Porphyritic monzonitic granite	Zircon	LA-MC-ICP-MS U-Pb	34.68–36.64	Deng et al., 2015
	Quartz syenite porphyry	Zircon	LA-MC-ICP-MS U-Pb	34.92±0.66	He et al., 2012
	Quartz syenite porphyry	Zircon	LA-MC-ICP-MS U-Pb	35.00±0.17	This study
Hongnitang rock body	Quartz syenite porphyry	Zircon	LA-MC-ICP-MS U-Pb	36.24±0.63	He et al., 2012
	Quartz syenite porphyry	Zircon	LA-MC-ICP-MS U-Pb	36.48±0.26	He et al., 2013
	Quartz syenite porphyry	K-feldspar	Ar-Ar	25.89±0.13	Xu et al., 2006
	Quartz syenite porphyry (surface)	K-feldspar	Ar-Ar	25.89±0.13	Ying et al., 2004
	Quartz porphyry	Plagioclase	Ar-Ar	24.56±0.06	Wang et al., 2001
Dashadi rock body	Quartz syenite porphyry	Zircon	LA-MC-ICP-MS U-Pb	35.06±0.16	This study
	Quartz monzonite porphyry	Zircon	LA-MC-ICP-MS U-Pb	36.72±0.25	This study
Dashadi rock body	Monzogranite porphyry	Zircon	SHRIMP U-Pb	35.40 ± 0.50	Wang et al., 2016

2016). The two-stage Hf zircon model age is approximately 1.0 Ga (He, 2014), which is consistent with the age of the new crust of the Neo-proterozoic Yangtze craton (Wang et al., 2012), indicating that the new component is probably the basic component of Neo-proterozoic.

Lead isotope variations in the porphyry are relatively small. Values of  $^{206}\text{Pb}/^{204}\text{Pb}$ ,  $^{207}\text{Pb}/^{204}\text{Pb}$ , and  $^{208}\text{Pb}/^{204}\text{Pb}$  are 18.691–18.931, 15.664–15.703, and 38.898–39.124, respectively. The  $(^{87}\text{Sr}/^{86}\text{Sr})_i$  composition is 0.70753–0.70862, and the  $\varepsilon_{\text{Nd}}(t)$  composition varies from –6.87 to –8.60. The two-stage depleted-mantle Nd model age ( $t_{\text{DM2}}$ ) is from 1.4 to 1.5 Ga, indicating that diagenetic materials were derived from the lower crust (Wang et al., 2016).

The rock body has low  $(\text{Dd}/\text{Lu})_{\text{N}}$  ratios as well as high  $\text{Sr}/\text{Y}$ ,  $(\text{La}/\text{Yb})_{\text{N}}$ , and  $(\text{Dy}/\text{Yb})_{\text{N}}$  ratios, indicating that the rock body originated from the partial melting of a hornblende–garnet source region. The quartz syenite and quartz monzonite porphyry also have similar Sr, Nd, and Pb isotopic compositions with amphibolite xenoliths in Eocene acidic rocks from the western Yunnan province. Sulfur isotopic compositions of the alkali-rich porphyry bodies (1.0–2.5‰) are similar to deep mantle sulfur compositions ( $0 \pm 3\%$ ; Hoefs, 1997), indicating that the rock body is partially derived from a deep mantle magma. Therefore, the rock bodies likely originated from the thickening of the lower crust with a hornblende–garnet facies and may have been affected by the upwelling of the lithospheric mantle.

Rock bodies were emplaced between  $34.62 \pm 0.25$  and  $36.72 \pm 0.25$  Ma, a period of dynamic tectonic transition after the collision of the India and Eurasian blocks (Zhang Hongrui and Hou Zenqian, 2015). The ore district is part of the Jinsha River–Ailao Mountain alkali-rich porphyry belt (40–35 Ma) that formed via strong crust-mantle

interaction. The alkali-rich porphyry metallogenic belt is located in the back arc extension zone of the Myitkyina collision zone (the southern extension of the Gangdese collision zone). During the collision process, alkali-rich porphyry magma, formed by the partial melting of metasomatized mantle along the Jinsha River–Red River strike slip fault zone, locally intruded upward and differentiated to form the Beiya-bearing Cu–Au–Mo porphyry-type metallogenic belt (Mao et al., 2017).

#### 4.1.2 Relationship between alkali-rich porphyry and mineralization

There is a close spatial relationship between the Au–polymetallic deposits and the rock bodies, in which the ore bodies, with different types of mineralization, occur as rings around the rock bodies. The contents of Au, Fe, Ag, Cu, Pb, Zn, and other elements in the rock body are generally several times higher than the average values of syenite and granite in China (Tables 4–5). Compared with the Wangdongshan and Hongnitang rock bodies, the Dashadi rock body, a major source of ore-forming elements, is characterized by relatively well-developed Cu (Mo) mineralization, a lack of Au mineralization and enrichments in Cu (3.6–2254 ppm), Mo (2.91–24 ppm), and other trace elements related to metallogeny. The rock-forming age of the porphyries is between 34.62 and 36.72 Ma, which agrees with the ore-forming age ranging from 36.46 to 39.44 Ma.

The genesis of the deposit is closely related to the alkaline intrusive rocks, because the alkali-rich porphyry is the source of ore-forming materials and fluids, which is supported by the following evidence:

(1) REE distribution patterns for many types of gold ore samples, from the deposits, are consistent with the quartz monzonite and quartz syenite porphyries. On REE pattern diagrams, the REE distribution curves for all samples are

**Table 4 Trace elemental results related to mineralization in the main ore-forming rocks in the Beiya Au–polymetallic deposit**

Ore-forming element	Wangdongshan rock body (Quartz syenite porphyry)			Hongnitang rock body (Quartz syenite porphyry)			Dashadi rock body (Quartz monzonite porphyry)			Syenite in China
	Min.	Max.	Mean (piece)	Min.	Max.	Mean (piece)	Min.	Max.	Mean (piece)	Mean
Au (ppb)	0.80	1070	167.20(20)	0.25	32.3	7.04(15)	6900	21200	9430(6)	0.53
Ag (ppb)	236	8830	1844(20)	1420	11700	3513(15)	30	2310	630(6)	0.057
Cu (ppm)	44.1	390	147.91(13)	5.26	184.49	63.94(5)	3.60	2254	411.48(9)	15
Pb (ppm)	15.60	650	116.65(18)	43.44	756.13	320.83(8)	26.94	28.57	27.76(2)	31
Zn (ppm)	30.8	143	59.26(13)	11.36	57.55	34.76(5)	14.1	184	97.22(9)	76
Mo (ppm)	0.832	154	14.30(13)	0.05	12.6	5.88(15)	2.91	24.0	10.52(9)	0.9
Sb (ppm)	0.278	1.84	1.06(13)	2.32	30.00	14.56(15)				0.22
Bi (ppm)	0.105	2.45	0.759(13)	0.15	173	18.37(15)				0.17
As (ppm)	2.31	269	37.98(20)	32	1800	512.6(15)				1.2
Cd (ppm)	0.08	1.38	0.42(20)	0.52	1.90	1.01(15)				0.09
Data source	Data of Au, Ag, As and Cd from Yang et al., 2015; data of Cu, Zn, Mo, Sb and Bi from Deng et al., 2015a and Liu et al., 2015; data of Pb from this paper and Deng et al., 2015a			Data of Au, Ag, Mo, Sb, Bi, As and Cd from Yang et al., 2015; data of Cu and Zn from Deng et al., 2015a and Liu et al., 2015; data of Pb from this paper and Deng et al., 2015a			Data of Au and Ag from Wang et al., 2016; Data of Cu, Zn and Mo from Wang et al., 2016 and He, 2014; Data of Pb from this paper			Yan et al., 1996

consistent, with LREE-enriched and HREE-depleted right-inclined smooth curves indicating that the genesis of the Au–polymetallic deposit is closely related to the two types of intrusive bodies. The PGE characteristics of the samples from the skarn-type Au and hydrothermal Au deposit, in the outer zone, indicate that the alkali-rich porphyry supplies the Au (Jiang et al., 2015).

(2) The  $\delta^{34}\text{S}$  sulfide values for ore deposits range from  $-3$  to  $+1\text{‰}$  and are mostly between  $-1$  and  $0\text{‰}$ , with tower distribution characteristics, indicating that the sulfur source is highly homogeneous (Zhou et al., 2016). Sulfur isotopic data for hydrothermal Pb–Zn–Ag and Au deposits in stratoid and vein form, from the Qin River ore section in the remote zone, vary from  $-2.4$  to  $+2.8\text{‰}$ , indicating that the source is uniform and that its range is narrow. The sulfur isotopic composition of the alkali-rich porphyry body ( $1.0$ – $2.5\text{‰}$ ) is basically the same. The sulfur isotopic composition of sulfide in this deposit is similar to that of the deep source sulfur ( $0\pm 3\text{‰}$ ; Hoefs, 1997), indicating that the deposit has the same sulfur source (magmatic sulfur) as the alkali-rich porphyry and that mineralization is closely associated with magmatic hydrothermal fluids.

(3) The  $^{206}\text{Pb}/^{204}\text{Pb}$  ore values are  $18.626$ – $18.699$ , with an average of  $18.653207$ ; the  $^{207}\text{Pb}/^{204}\text{Pb}$  values are between  $15.642$  and  $15.725$ , with an average of  $15.682$ ; and the  $^{208}\text{Pb}/^{204}\text{Pb}$  values are  $38.892$ – $39.180$ , with an average of  $39.029$  (Wu Song and Li Wenchang, 2015). Porphyry Pb isotopes in the ore district are nearly identical. On the Pb isotopic composition diagram, both Pb from ores throughout the different deposits and sections and Pb from the alkali-rich porphyry are very similar indicating that their initial source is similar and that the formation of ore-forming fluids may be related to fractional crystallization in the alkali-rich porphyry.

The above results indicate that the S and Pb isotopic compositions of the ores are in good agreement with the alkali-rich porphyry in the ore district. This reveals that the source of ore-forming materials is related to deep magma. Previous studies using Pb isotopes found that almost all ore-forming materials are associated with fluids separated by alkali-rich magma, and most of them are directly derived from the source area of the alkali-rich magma.

#### 4.1.3 Comparison of various rock bodies

Results on the Himalayan alkali-rich porphyry bodies or lamprophyry in the ore district and the surrounding area indicate that the petrological characteristics of the mineralized and non-mineralized rock bodies are basically the same, especially for the quartz syenite and quartz monzonite porphyry (monzogranite porphyry), and their constituent minerals, texture, structure, as well as major,

trace, and rare earth element contents exhibit obvious consistency (Zhou et al., 2016).

Compared with the other five small rock bodies without mineralization in the ore district, potassium silicate alteration is strong with certain instances of pyritization in the interior of the Wangdongshan, Hongnitang and Dashadi rock bodies. The contents of Au, Fe, Cu, Pb, Zn, and Ag are higher in the mineralized intrusions, which also display lower Al, Fe and Mg contents. This is a possible cause for insignificant strong mineralization in the five small rock bodies.

#### 4.2 Ore-forming wall rocks (Middle Triassic Beiya Fm. ( $T_2b$ ) carbonate rocks)

Impure carbonate rocks ( $T_2b$ ) from the Middle Triassic Beiya Formation provide favorable surrounding conditions and hosting space for the formation of deposits, i.e. the strata necessary for skarn formation.

According to lithological associations, the Middle Triassic Beiya formation ( $T_2b$ ) can be divided into five lithologic members from the bottom to up: 1)  $T_2b^1$  is a light gray, middle-layered reticulate, banded argillaceous fine-grained limestone and breccoid-like limestone, occasionally intercalating thin middle-layered arkosic sandstone, with a thickness of  $33$ – $112$  m; 2)  $T_2b^2$  is a gray–dark gray, middle thick-bedded breccoid-like argillaceous fine-grained limestone, with a thickness of  $30$ – $156$  m; 3)  $T_2b^3$  is a light gray, middle thick-bedded argillaceous limestone, locally intercalating banded limestone, with a thickness of  $25$ – $165$  m; 4)  $T_2b^4$  is a middle thick-layered, rhythmic interlayer of gray breccoid dolomite and banded dolomite, locally intercalating gray iron calcarenite, containing dolomitic calcarenite and lump limonite (an important ore-bearing horizon), with a thickness of  $30$ – $156$  m, and 5)  $T_2b^5$  is a gray-off–white, middle thick-bedded dolomitic calcarenite and dolomite, with strong, broken alteration and weathering, typically occurring as brown sucrosic, with a thickness of  $45$ – $107$  m.

The Beiya formation is a suite of impure carbonate rocks, especially vermicular argillaceous limestone and bioclastic limestone ( $T_2b^3$ ), iron limestone ( $T_2b^2$ ), and dolomitic calcarenite ( $T_2b^5$ ), with active chemical properties, developed karst structures, as well as rigid mechanical properties and performance. Under stress, it is not easily deformed and forms, instead, structural fissures and interlayer fracture zones that are favorable for mineralization, acting as channels for an ore-forming fluid or space for mineral precipitation. In the porphyry contact zone, ore-bearing hydrothermal fluids replaced carbonate rocks to form skarn type Au–Fe ore bodies. Away from the porphyry, the ore-bearing hydrothermal fluid

penetrated along the structural fissures and interlayer fracture zones to form stratoid and vein Au–Fe ore bodies.

### 4.3 Metallogenic structures

The SN Beiya syncline, fracture, and interlayer fracture formed during the early Yanshan–Himalayan period as well as the contact zone formed by the emplacement of alkali-rich porphyries in the middle Himalayan period comprise the important metallogenic structures. The Beiya syncline, the secondary structure of the west limb of the SN Heqing–Songgui wide and gentle compound syncline, SN faults (F1, F2, F3, F4, F5, and F6), EW faults (F22, F25, and F26), NE fault (F27), and NW faults (F21 and F28) (Fig. 1) belong to the pre-metallogenic and metallogenic structures. The NNW shear fault and the SN low-angle overthrust fault, developed in  $N_2s$  strata since the Quaternary period, are the post-metallogenic structures.

The main fold structure in the ore district is the SN Beiya syncline, located on the southern tilting end of the Songgui compound syncline, which belongs to a secondary structure of the Heqing–Songgui compound syncline. The Beiya syncline is closed north of the Shuijing and south of the Jimingsi–Guanyinjing areas, with an axial length of nearly 12 km and a width between two limbs of 1.2–1.8 km. The Beiya syncline is a wide and slow brachy syncline with an axial direction of NNE. The outcropped stratum in the west limb is  $T_2b^{1-5}$ , inclined to the east at a dip angle of 30–60°. The east limb contains  $T_2b^{1-5}$ ,  $T_1q$ , and  $P_2\beta$ , inclined to the west at a dip angle of 10–40°. Local sections in the two limbs were influenced by faults and a magmatic intrusion, developing secondary folds, faults, joints, and fissures. The occurrence of the core is flat, formed by the SN Beiya intermontane basin and covered by the Pliocene Sangying Formation. Wandongshan was influenced by the emplacement of the Wandongshan rock body to form a SN secondary anticline in the upper part and two sides of the rock body, a SN syncline fold on both sides (Fig. 2a), with an axial length

of 800–1,000 m, and a width in the EW direction of 500–800 m.

There are two main groups of faults in the ore district: one group of nearly north–south and another group of nearly EW, as well as minor NE and NW faults in the two groups, located in the core and both limbs of the Beiya syncline. The nearly SN fault group is a rock-control and ore-control fault (pre-metallogenic or metallogenic period) in the ore district, mainly including the F1, F2, F3, and F4 of the east limb as well as F6 and F5 of the west limb. The F6 and F5 are thrust faults occurring in the shallow, flat and deep steep. F2, F3 and F4 are the steep compressive faults on the hanging side of the F1 fault, and rocks from the hanging wall and footwall have different degrees of breakage and alteration. The stratoid, lentoid and vein ore bodies occur in parallel along the fissure fracture zone, indicating that the faults are the main ore-control and ore-host structures in the ore district, with characteristics of multi-period activities. Near EW faults are transtension transverse faults such as F22, F25, and F26, whereas NE and NW faults are transpressional shear lateral faults such as F21, F27 and F28. Multi-period activities displaced and destroyed the strata, rock, ore body as well as early faults and later lamprophyre dikes that were intruded along the faults.

### 4.4 Weathering-accumulation-type (paleo-weathering crust-type) Fe–Au deposit

The weathering-accumulation-type (paleo-weathering crust-type) Fe–Au deposit occurs in predominantly polymictic Au–limonite-bearing sand gravel and claystone from alluvial and lacustrine deposition in the bottom of the lower Miocene Sanying formation ( $N_2s$ ), where the upper part is gray limy breccia bodies formed by a gliding nappe. This suite of strata forms an angular unconformable contact with the overlying carbonate rocks of the Beiya formation ( $T_2b$ ), formed during the Middle Triassic period, whereas the alkali-rich porphyry and skarn -type Au–Fe ore body formed during the Himalayan

**Table 5 Trace element results of other ore-forming rock bodies in the Beiya Au–polymetallic deposit**

Ore-forming element	Matouwan rock body			Bailiancun rock body	Weiganpo rock body	Bijiashan rock body	Yanshuijing rock body	Putaihan rock body	Unknown rock body	Syenite in China
	Min.	Max.	Mean (piece)	Mean (piece)	Mean (piece)	Mean (piece)	Mean (piece)	Mean (piece)	Mean (piece)	Mean
Au (ppb)	0.025	2.92	0.71(17)					1.56(20)	0.62(7)	0.53
Ag (ppb)	30.0	2460	399.6(17)					107.6(20)	28.10(7)	0.057
Cu (ppm)	5.10	652	176.34(18)	4.12(2)	51.23(1)	7.28(8)	7.98(1)	27.95(20)	6.66(7)	15
Pb (ppm)	25.40	143	56.89(18)	233.51(2)	51.64(1)	37.16(8)	47.93(1)	33.80(20)	14.76(7)	31
Zn (ppm)	17.1	84.5	45.24(18)	64.67(2)	125.29(1)	265.0(8)	44.70(1)	30.64(20)	21.07(7)	76
Mo (ppm)	0.26	4.35	1.17(17)					2.04(20)	0.35(7)	0.9
Sb (ppm)	0.26	9.12	1.38(17)					5.36(20)	0.23(7)	0.22
Bi (ppm)	0.03	2.23	0.29(17)					3.10(20)	0.12(7)	0.17
As (ppm)	0.40	29.1	5.65(17)					5.62(20)	5.10(7)	1.2
Cd (ppm)	0.03	0.80	0.26(17)					0.14(20)	0.04(7)	0.09
Data source	Yang et al., 2015; added data of Cu, Zn and Pb analyzed in this paper			This paper		Xu et al., 2007	Wu et al., 2005	Yang et al., 2015		Yan et al., 1996

period. The ore bodies are distributed in a relatively low-lying depression near the axis of the Beiya basin, with a large extension along the SN axis, up to 1,840 m; a maximum thickness, near the axis, of 10–35.32 m; and a higher grade (2.00–20.24ppm Au). On both sides of the EW direction basin, the extension is relatively narrow with a width of 420–500 m, a small thickness, a reduced grade, and a rapidly changing local section. The geological characteristics of the ore bodies are listed in detail in Tables 1 and 6 as well as Figure 2a. Since the Beiya is cut by biotite syenite porphyry veins, with an isotopic age of 3.8–3.6 Ma (Xu et al., 2006), the depression-sedimentation of the Cenozoic Beiya intermontane basin occurred during the period from (35–36.72) to 3.8 Ma.

The geological characteristics of the ore bodies indicate that primary Au ore bodies and Au-bearing altered rocks experienced hypergenesis and transformation, and then migrated to the Beiya mountain basin to accumulate and form the weathering-accumulation-type Au deposit. The deposits formed over long periods and with diversity, mostly occurring in the negative terrain near the primary ore body.

#### 4.5 Ore-controlling factors

##### 4.5.1 Alkali-rich porphyry and wall rock

(1) The alkali-rich porphyry and the wall rock controlled the spatial distribution of polymetallic deposits.

In the Wandongshan ore section, the mineralized zoning of the rock body interior, the skarn zone, and the distal contact zone formed around the Wandongshan rock body. The small and enriched ore bodies occurred as lenticulars and veins in the steep fissures in the rock body. Near the contact zone of the rock body, the contact-zone-type ore bodies such as KT52 formed along the contact skarn zone between the rock body and the Middle Triassic Beiya formation ( $T_2b$ ) carbonate rocks and were then distributed intermittently around the rock body on the horizontal section. In the EW exploration line section, the ore body is tilted to the west with an irregular inverted "U" shape, whose top part has been eroded. Only the ore body on the upper and lower contact zones has been preserved. In the southern turning point for the emplacement of the rock body (exploration lines 54–50 in the South), the thickness of the skarn belt around the rock body is large and that of the ore body is the largest (the maximum vertical thickness is more than 150 m). In the outer zone, far away from the rock body-distal zone, stratoid ore body (I, II and III ore bodies from the Qinhe ore section as well as the KT32 ore body from Weiganpo ore section) in the interlayer fracture zone as well as vein and lenticular ore bodies in the faulted fracture zone are developed. The rock body was emplaced in the 600 m range between

exploration lines 50 and 80. The ore body in the contact zone is located in the 0–500 m area around the rock body, and that in the outer belt-distal zone is 1–5 km from the rock body (Table 6).

The KT10, KT11, and KT12 ore bodies are controlled by the Hongnitang rock body that occurred in the contact skarn zone in the upper and lower plates of the rock body, distributed between exploration lines 31 and 111, whose controlled length is 1,600 m, width is from 74 to 813 m, and extension depth is between 80 and 824 m, with a distributive elevation of 1,781.80–2,116.46 m and a buried depth of 0–429 m. Between exploration lines 31 and 79 in the north, the ore body moves towards the SN direction and generally tilts to the west. Between exploration lines 79 and 111 in the south (Jingouba ore section), the ore body occurs along the interlayer fracture zone of  $T_2b$  and dips to the east.

The KT17 and KT18 ore bodies are controlled by the Dashadi rock body that occurs along the east contact zone of the rock body with the presence of steep slopes, distributed between exploration lines 35 and 69, with a controlled length of 600 m, a controlled depth from 80 to 824 m, and a distributive elevation between 1,781 and 2,116 m. In the Middle Triassic Beiya formation ( $T_2b$ ) carbonate rocks between Hongnitang and Dashadi rock bodies, KT13 and KT15, are ore bodies that occurred along the interlayer fracture zone.

Currently, the ore bodies discovered in reconnaissance are distributed mainly in the Middle Triassic Beiya formation ( $T_2b$ ) carbonate rocks. There are no industrial ore bodies in the underlying upper Permian basalt formation ( $P_2\beta$ ) basalt intercalating tuff, the contact zone between the rock body and lower Triassic Qingtianbao formation ( $T_1q$ ) sandy conglomerate and sandstone or strata. The alkali-rich porphyry intrusive bodies and Middle Triassic Beiya formation ( $T_2b$ ) carbonate rocks control the range of distribution of the polymetallic deposits spatially.

(2) The alkali-rich porphyry bodies control the spatial zonation of the mineralization type of the porphyry hydrothermal metallogenic system.

The ore-controlling regularity of the Wandongshan rock body is represented by ore zonation from the hydrothermal Cu–Au ore body to the skarn-type Au–Cu–Fe ore body to the skarn-type Au–Fe ore body to the hydrothermal Au–Fe–Pb ore body to the hydrothermal Pb–Ag ore body with the location from the rock body to the contact zone to carbonate formation (outer zone to distal). The ore-controlling regularity of the Hongnitang rock body is represented by ore zonation from the skarn-type Au–Fe–Cu ore body to the skarn-type Au–Fe–Pb ore body to the hydrothermal Au–Pb–Ag ore body with the location from

Table 6 Metallogenic geological characteristics of each ore section in the Beiya gold-polymetallic deposit

Ore section	Wandongshan ore section	Qinhe ore section	Hongnitang ore section (west)	Hongnitang ore section (east)	Jingouba ore section	Weigapo-Bijiaoshan ore section	Yangjiayuan ore section	Bailiancun ore section
Geology	Located near the core of the Beiya syncline in the northern ore district, it presents as compound secondary syncline. Outcropped strata are $T_2b^{4-5}$ dolomite, dolomitic limestone and $N_{2s}$ sand-mudstone. Structures are NNW-Beiya-Qinhe syncline, well-developed interlayer fracture zone and NW-trending $F_{23}$ fault in the southern part. Small veins of quartz syenite porphyry occur EW-trending fault.	It is located at the northernmost end of the ore district and outcropped strata are $T_2b^{4-5}$ argillaceous limestone and dolomitic limestone. Neogene Sanying Fm. $N_{2s}$ sand-mudstone. Structures are NNW-Beiya-Qinhe syncline, well-developed interlayer fracture zone and NW-trending $F_{23}$ fault in the southern part. Small veins of quartz syenite porphyry occur sporadically.	It is located in the west limb of the Beiya syncline in the central part of the ore district, and the outcropped strata are $T_2b^{4-5}$ dolomite and dolomitic limestone. SN-trending $F_5$ and EW-trending $F_{25}$ , $F_{22}$ and $F_{23}$ . Hongnitang quartz syenite porphyry body occurs along the junction among $F_5$ , $F_{22}$ and $F_{23}$ .	It is located in the core of the Beiya syncline in the central part of the ore district, with outcropped strata of $T_2b^{4-5}$ dolomite, dolomitic limestone and $N_{2s}$ sand-mudstone. SN-trending $F_5$ and EW-trending $F_{25}$ , $F_{22}$ and $F_{23}$ . Dashiadi buried quartz monzonite porphyry distributes along $F_6$ fault.	It is located in the core and west limb of the Beiya syncline in the south part of the ore district, with outcropped strata of $T_2b^{4-5}$ dolomite and dolomitic limestone. SN-trending $F_5$ and EW-trending $F_6$ and $F_{21}$ . Small veins of quartz syenite porphyry occur sporadically, and lamprophyre veins occur along $F_{21}$ fault.	It is located in the east limb of the Beiya syncline in the central part of the ore district, with outcropped strata of $T_2b^{4-5}$ dolomite and dolomitic limestone. SN-trending $F_1$ , $F_2$ , $F_3$ and $F_4$ and EW-trending $F_{21}$ . Bijiaoshan and Guogaihan quartz monzonite porphyry bodies occur in $F_2$ and $F_1$ faults.	It is located in the west limb of the Beiya syncline in the central part of the ore district, with outcropped strata of $T_2b^{4-5}$ dolomite and dolomitic limestone. EW-trending $F_{25}$ , $F_{22}$ and $F_2$ as well as near SN-trending $F_{13}$ .	It is located in the east limb of the Beiya syncline in the northeastern part of the ore district, with outcropped strata of $T_2b^{4-5}$ basalt intercalating tuff. NW-trending $F_{28}$ . Bailiancun quartz monzonite porphyry body exposed here.
Ore-bearing rocks	Wandongshan quartz syenite porphyry	Wandongshan quartz syenite porphyry	Hongnitang quartz syenite porphyry	Dashiadi quartz monzonite porphyry	Hongnitang quartz syenite porphyry	Dashiadi buried quartz monzonite porphyry	Hongnitang quartz syenite porphyry	Bailiancun quartz monzonite porphyry
Metallogenic type and zoning	Hydrothermal vein-type Au-Fe-(Pb-Zn) mineralization in fissures and fractures; skarn-type Au-Fe-Cu mineralization in contact zone of porphyry body, hydrothermal vein type and paleo weathering crust type Au-Fe mineralization in interlayer or faulted fracture zone	Hydrothermal type layered Pb(Ag)-Au-Zn mineralization in interlayer fracture zone	Skarn-type Au-Fe-Cu(Pb-Zn) mineralization in contact zone of porphyry body, skarn-type Fe-Cu mineralization in interlayers	Skarn-type Fe-Cu (Mo) mineralization in contact zone of porphyry body, skarn-type Fe-Cu mineralization in interlayers, paleo weathering crust type Au-Fe mineralization	Skarn-type Au-Fe-Cu (Pb-Zn) mineralization in interlayers, hydrothermal vein-type Au-Fe-Cu (Pb-Zn) mineralization in faulted fracture zone	Hydrothermal vein-type Au and Pb-Zn-Ag mineralization in interlayers or faulted fracture zone	Hydrothermal vein-type Au and Pb-Zn-Ag mineralization in interlayers or faulted fracture zone	Skarn-type thin-vein Au (Pb-Ag) mineralization in the interlayer of steep shear fracture zone
Alteration type	Skarnization, silicification, marbleization, chloritization and carbonatization	Silicification, skarnization, decalcification of carbonate rocks, pyritization, magnetitization, chloritization, hornfelsization and carbonatization	Silicification, carbonatization and hornfelsization	Silicification, skarnization and hornfelsization	Silicification, skarnization, pyritization, chloritization, sideritization and carbonatization	Silicification, limonitization and carbonatization etc.	Silicification, limonitization and carbonatization	Silicification and limonitization
Occurrence position of ore body	Ore bodies in the contact zone of the rock body, fracture and fissure in the interior of the rock body, $T_2b^{4-5}$ interlayer or faulted fracture zone are about 0–500 m away from the rock body. Eluvial type ore body on the paleo weathering crust distributes in the periphery of the axis of the Beiya basin with relative large thickness of $N_{2s}$ .	Ore body in $T_2b^{4-5}$ interlayer fracture zone in distal zone is about 400–2700 m away from the northern boundary of the Wandongshan rock body	Ore body in the contact zone of the rock body is about 0–50 m away from the rock body, and skarn type ore body in $T_2b^{4-5}$ interlayer is about 0–500 m away from the rock body.	Ore body in the contact zone of the rock body is about 0–50 m away from the rock body, and skarn type ore body in $T_2b^{4-5}$ interlayer is about 0–300 m away from the rock body.	Ore body in $T_2b^{4-5}$ interlayer fracture zone is 500–1000 m away from Dashiadi buried rock body.	Ore body in $T_2b^{3-4}$ interlayers and faulted fracture zone in the outer zone is 500–1500 m away from Wandongshan and Dashiadi buried rock bodies.	Ore body in $T_2b^{4-5}$ interlayers in the outer zone and $F_{13}$ faulted fracture zone is 1000–2500m away from Hongnitang rock body.	Ore body in steep shear fracture zone in distal zone is 4000–5000 m away from Wandongshan and Hongnitang rock bodies.

Continued Table 6

Ore section	Wandongshah ore section	Qinhe ore section	Hongnitang ore section (west)	Hongnitang ore section (east)	Jingouba ore section	Weiganpo-Bijiqashan ore section	Yangjiayuan ore section	Bailiancun ore section
Main ore bodies	The ore bodies in the contact zone are mainly KT52 and its branch ore bodies. The ore bodies in interlayers or faulted fracture zone include KT63, KT43, KT46, KT49 (in the interior of the rock body), KT54-57, etc. Eluvial type ore bodies are KT4B, KT1, KT3 and KT5 and so on. The characteristics of the representative ore bodies are shown in Table 1.	24 Pb-Au(Ag) industrial ore bodies are controlled by the I, II, III and IV Au-Pb polymetallic ore belts, and occur in near horizon, with strike of NW, length of 129-2175 m, width in NE direction of 80-505 m, average thickness of 1.35-14.25 m and average grade of Pb 3.42%, Au 4.35ppm, Ag 42ppm, TFe 31.86% and Zn 0.95%.	The ore bodies in the contact zone are KT10-12, and the interlayer skarn type Fe-Cu ore bodies are KT3 and KT5. The characteristics of the representative ore body are shown in Table 1.	The ore bodies in the contact zone are KT17-19. Eluvial type ore bodies are KT4A-KT4E, KT1, KT3 and KT5 and so on. The characteristics of the representative ore bodies are shown in Table 1.	The ore bodies are KT10-11, with length along strike of 640 m, width of 80 m-496 m, thickness of 0.98 m-8.37 m, average thickness of 2.74 m and grade of Au 2.96ppm, Ag 152.4ppm, TFe 39.16%, Pb 5.76% and Zn 8.73%	The discovered ore bodies are KT-33 and KT35, with length along SN strike of 60-217 m, width in NE direction of 91-165 m, average thickness of 3.17-16.11 m and average grade of Pb 0.57%, Ag 65.67ppm, TFe 40.12%, Zn 2.41% and Au 2.31ppm.	The ore bodies discovered are V-1Pb and V-1Au/Ag PbFe, with steep dip, strike of NW, length of 435-450 m, extension depth in NE direction of 160-200 m, average thickness of 0.2-1.5 m and grade of Au 0.54-19.83ppm, with an average value of 3.22ppm.	Nine ore veins have been discovered, such as KT3, KT7-9, with NW strike, length of 160-170 m, extension depth of 40-200m, thickness of 0.2-1.5 m and grade of Au 0.54-19.83ppm, with an average value of 3.22ppm.
Ore minerals	Magnetite, pyrrhotite, pyrite, chalcopyrite, siderite, hematite, galena, sphalerite, limonite and cerussite.	Metallic minerals: galena, siderite, limonite, cerussite, sphalerite, pyrrhotite, natural gold, etc.	Magnetite, hematite, pyrite, chalcocopyrite, molybdenite and galena.	Magnetite, hematite, pyrite, chalcocopyrite, molybdenite and galena.	Magnetite, pyrrhotite, siderite, hematite and galena.	Galena, siderite, limonite and cerussite etc.	Galena, siderite, cerussite, natural gold, limonite, etc.	Pyrite, natural gold, and limonite etc.
Gangue minerals	garnet, diopside, chlorite, epidote, calcite, dolomite and quartz.	Calcite, quartz, and dolomite and so on.	Calcite, dolomite, quartz, feldspar, garnet, and epidote	Quartz, feldspar, diopside, chlorite, epidote, and kaolin	Calcite, dolomite, quartz, feldspar, and epidote.	Calcite, quartz and dolomite etc.	Calcite, quartz, and dolomite and so on	Calcite and quartz and so on
Texture and structure	Granular, metasomatic relict and poikilitic textures, and veinlet, disseminated, porphyritic, colloidal structures:	Granular, metasomatic relict and poikilitic textures, and veinlet, disseminated, porphyritic, colloidal structures:				Granular, metasomatic relict and poikilitic textures, and veinlet, disseminated, veinlet, porphyritic and colloidal structures.	Granular, metasomatic relict and poikilitic textures, and veinlet structures.	Granular, metasomatic relict and poikilitic textures, and veinlet structures
Resources/reserves	Au 254.574 t with a grade of 2.73ppm; Pb-Zn 189.67×10 <sup>4</sup> t with a grade of 1.56%; Ag 579.217 t with a grade of 35.01ppm; Cu 47.51×10 <sup>4</sup> t with grade of 0.57%; Fe ores 4748.15×10 <sup>4</sup> t with a grade of 32.17%	Pb 64.1257×10 <sup>4</sup> t; Au 1745kg; Ag 107.5 t; TFe ores 557.98×10 <sup>4</sup> t; Associated Pb 1.1948×10 <sup>4</sup> t; Au 13303 kg; Ag 9116.0t; Zn 9.891×10 <sup>4</sup> t; Cu 1.5434×10 <sup>4</sup> t; TFe ores 604.43×10 <sup>4</sup> t	Au 38.167 t with a grade of 2.27ppm; Pb+Zn 57.57×10 <sup>4</sup> t with a grade of 3.79%; Cu 5.15×10 <sup>4</sup> t with a grade of 0.49%; Fe ore 2488.6×10 <sup>4</sup> t with grade of 33.21%; Mo 3782 t with a grade of 0.047%	Au 3849 kg; Ag 480t; Fe ores 327.4128×10 <sup>4</sup> t; Pb+Zn 16.14×10 <sup>4</sup> t	Au 3849 kg; Ag 480t; Fe ores 327.4128×10 <sup>4</sup> t; Pb+Zn 16.14×10 <sup>4</sup> t	Pb-Zn: 14.17×10 <sup>4</sup> t; Fe ores 43.46×10 <sup>4</sup> t; Ag 16.46 t; Au 408 kg	Pb 5.64 × 10 <sup>4</sup> t; Au 2744 kg; Ag 122.6 t; TFe ores 46.46× 10 <sup>4</sup> t	Au 0.621 t

the contact zone of the rock body to carbonate formation (outer zone to distal). That of the Dashadi rock body is represented by ore zonation from the porphyry-type Cu–Au to skarn-type Cu (Mo)–Fe to hydrothermal Au and Pb–Ag in turn with the location from the rock body to peripheral strata. The skarn Fe–Cu ore bodies formed in the interlayer fracture zone of carbonate rocks ( $T_2b$ ) between Dashadi and Hongnitang rock bodies.

(3) The alkali-rich porphyry bodies control the spatial zonation of the alteration type of the deposit.

Alteration occurs in the contact zone between the rock body and the surrounding rock, the interlayer fracture zone of carbonate formation ( $T_2b$ ), or the faulted fracture zone in the strata, including two alteration-mineralized zones that are the inner and outer contact zones. From the rock body to the contact zone to the carbonate formation (the outer zone to the distal), alteration types include self-metamorphic potassic alteration of the rock body, silicification to epidotization and diopsidization in the internal contact zone, then garnetization and diopsidization of the surrounding rock occurs in the outer contact zone, and later chloritization and carbonatization.

(4) The contact modes and forms of the alkali-rich rock bodies and the surrounding rock control the occurrence, form and scale of the main ore bodies.

For the intrusion contact mode of the rock body gently inclined to the strata, the heat and ore fluid are not easily lost; this is beneficial to contact metasomatism. The mineralization scale of the contact zone of the Wandongshan rock body is larger than that of other skarn-type ore zones near the contact zone, which may be related to the contact mode. The position where contact relationship between intrusions and strata becomes gentle and the depressions formed by contact of the rock body are the most favorable parts for forming thick and large ore bodies. For example, KT52 Au–Fe polymetallic ore bodies discovered in exploration lines 50, 54, and 56, in the Wandongshan ore section, have a relatively large thickness, and between exploration lines 69 and 70, of the Hongnitang rock body, KT10 and KT11 ore bodies have the maximum thickness in the position where the contact zone changes from sharp to gentle. This is mainly due to contact mode increases in the contact area and the fact that the stress in the depression is small and the ore fluid is easily gatherable. The ore body becomes thinner in areas where the contact zone is sharp (Fig. 2).

The above-mentioned results indicate that the alkali-rich porphyries control the internal and external zoning structure of four mineralization styles, i.e. from vein Au–Fe (Cu) ore bodies in the interior of the rock body to the skarn-type Au–Fe (Pb–Cu) massive ore body in the contact zone to the stratoid and lenticular Pb–Ag–Au ore body in

interlayer fracture zone of the outer zone to vein Au–Pb–Ag ore body in the distal zone. The deposit belongs to the porphyry–skarn-type Au–Fe–Cu–Pb–Zn (Ag) polymetallic metallogenic system formed by the gradual evolution of magmatic differentiated hydrothermal solutions.

#### 4.5.2 Structures on mineralization

The structures in the ore district and geological characteristics of the deposit indicate that Au–polymetallic ore bodies in the ore district occur in both limbs of the Beiya syncline, the contact fracture zone between the rock body and the wall rock, the axial part of the syncline where joints and fissures are well developed or interlayer fracture zone in the limb. This indicates that folds control the distribution of the rock (ore) bodies. The near SN faults in both limbs of the syncline control the distribution of porphyry (veins) bodies, and related Au–polymetallic ore bodies are the main rock-control and ore-control structures, the channels for magma intrusion and migration of the ore-forming fluid, as well as the main metallogenic structures and ore-hosted structures. The faults also control the scale, mineralization direction, and spatial distribution of the ore bodies. The matched secondary fractures and fissures directly control the form, occurrence, scale, and enrichment of the gold-bearing ore bodies. In the ore district, the contact fracture zone between the rock body and carbonate rocks, the tectonic fracture zone in the interlayer of carbonate layers as well as between carbonate and clastic rocks, and the section where fissures are well developed are the main hosts for ore bodies. The form and occurrence of the ore bodies agree with the contact of the rock body, the structural belt, the interlayer structural fracture zone, and the fissure zone.

#### 4.5.3 Weathering-accumulation-type Fe–Au deposit formed by supergenesis

The porphyry–skarn-type ore bodies in the contact zone, interlayer fracture-zone-type ore bodies, vein-shaped ore bodies in secondary fracture fissures related to the alkali-rich porphyries formed in the Himalayan period, and the form of the basement depression of the basin are the main ore-controlling factors for the weathering-accumulation-type (paleo weathering crust type) Fe–Au deposit formed by supergenesis.

After the formation of porphyry–skarn-type deposits, the Beiya area subsided and eroded throughout the Neogene to form the SN, narrow, small intermontane eroded depression basins at the center of Beiya, with a length, in SN direction, of 4–5 km and a width, in the EW direction, of 1–2 km. The wall rocks on the surface, in the shallow part of the basement of the basin, and the ore bodies experienced long-term weathering and denudation

to form uneven paleo-geomorphological features and developed Pliocene lacustrine deposition ( $N_{2S}$ ). In the depressed section above the unconformity, Fe–Au deposits accumulated and were preserved by the cover of lacustrine sediments.

## 5 Conclusions

(1) The emplacement of three alkali-rich intrusive bodies (the semi-buried Wangdongshan rock body, the buried Dashadi rock body, and the semi-buried Hongnitang rock body) formed between the late Eocene and the early Oligocene, resulting in the formation of the Beiya porphyry–skarn-type Au–polymetallic deposit.

(2) Alkali-rich porphyries consisting of quartz syenite and quartz monzonite porphyry belong to the alkaline metaluminous–peraluminous series (shoshonitic Series) formed during the Himalayan period. The porphyries have high  $SiO_2$  content, high (La/Yb) $N$  and (Dy/Yb) $N$  ratios, relatively low contents of MgO, Cr, Ni, Co, and V, relatively high Sr content and Sr/Y ratios, as well as a low (Dd/Lu) $N$  ratio and contents of Y and Yb, enriched in the LILEs and depleted in the HFSEs.

(3) The rock-forming ages of the main ore-forming porphyries are 34.62–36.72 Ma and are nearly identical to the ore-forming ages 36.46–39.44 Ma. The metallogenic rock body may originate from partial melting of the lower crustal material. The ascent and emplacement of magmas along the Jinsha River–Red River large strike-slip deep fracture zone and the secondary Ma'anshan fracture zone, formed by the oblique collision along Indian plate to Eurasian plate, led to the formation of the alkali-rich porphyries.

(4) Vein-shaped Au–Fe (Cu) ore body in the core of alkali-rich porphyry, skarn type Au–Fe (Cu–Pb) massive ore body in the contact zone, stratoid and lenticular Pb–Ag–Au ore body in interlayer fracture zone of the outer zone, and vein-shaped Au–Pb–Ag ore body in distal zone constitute the porphyry–skarn type Au–Fe–Cu–Pb–Zn (Ag)–polymetallic metallogenic system.

(5) Impure carbonate rocks from the Middle Triassic Beiya Fm. ( $T_2b$ ) provide favorable surrounding conditions and hosting space for the formation of deposits. The contact fracture zone between the rock body and carbonate rocks, tectonic fracture zone in the interlayer of carbonate layers and between carbonate and clastic rocks and the section where fissures are well developed are the main hosting positions for ore bodies.

(6) The metallogenic parent ores of weathering–accumulation-type (paleo weathering crust-type) Fe–Au deposits formed by supergene processes are the porphyry–skarn-type ore body and the interlayer fracture–zone-type

ore body, which is the vein-shaped ore body in secondary fracture and fissures formed early. The small intermontane eroded basin in the core of the Beiya syncline controlled the spatial distribution of ore bodies.

## Acknowledgments

Authors are sincerely grateful to Academician Mao Jingwen from the Institute of Mineral Resources, Chinese Academy of Geological Sciences and anonymous experts from editorial board for their great help and careful review of this paper. This study was jointly financially supported by “Yunling Scholars” Research Project from Yunnan Province, China Geological Survey Project (No. DD20160124 and 12120114013501), the National Natural Science Foundation of China (grant No. 41602103), and the “Study on metallogenic regularities and metallogenic series of gold–polymetallic deposits, Northwestern Yunnan Province” research project (E1107) from Yunnan Gold & Mining Group Co., Ltd.

Manuscript received Mar. 21, 2017

accepted Jan. 15, 2018

edited by Fei Hongcai

## References

- Cai Xinping, 1993. Characteristics, genesis and prospecting of Beiya gold deposit, western Yunnan. In: *Geology and Geochemistry of Gold Deposits in China*. Beijing: Science Press, 134–151 (in Chinese).
- Cai Xinping, Zhao Dashen and Liu Bingguang, 1991. *Characteristics, genesis and target prediction of Beiya gold deposit, western Yunnan*. Research Report of Institute of Geology of Chinese Academy of Science, 1–15.
- Chen Aibin, Sun Caixia, Jiang Hua and Yang Jianyu, 2011. Metallogenic prognosis based on comprehensive information in the Beiya gold deposit, Yunnan Province. *Geology and Exploration*, 47(4): 0633–0641 (in Chinese with English abstract).
- Cui Yinliang, Chen Xianshen and Yan Jianguo, 2001. Geological characteristics and metallogenic condition of lateritic clay-type gold deposits in Beiya. *Acta Mineralogica Sinica*, 21(4): 654–658 (in Chinese with English abstract).
- Cui Yinliang, Yan Jianguo and Chen Xianshen, 2003. A study of ore-prospecting signs and model. *Gold*, 24(7): 7–10 (in Chinese with English abstract).
- Cui Yinliang, Xu Heng, Zhou Jiayi, Zhang Miaohong, Jiang Yongguo and Zeng Min, 2017. Alkaline porphyries in the Chenghai–Binchuan tectono-magmatic belt, western Yunnan province, SW China. *Acta Geologica Sinica* (English Edition), 91(supp. 1): 74–75.
- Deng Jun, Yang Liqiang, Gei Liangsheng, Yuan ShiSong, Wang Qingfei, Zhang Jing, Gong Qingjie and Wang Changming, 2010. Character and post-ore changes, modify cations and preservation of Cenozoic alkali-rich porphyry gold metallogenic system in western Yunnan Province. *Acta Petrologica Sinica*, 26(6): 1633–1645 (in Chinese with

- English abstract).
- Deng Jun, Li Wenchang, Fu Degui, Yang Liqiang, He Zhonghua, Zhou Yunman, Zhang Jing and Ge Liangsheng, 2012. *Cenozoic gold metallogenic system in the southern section Sanjiang region, Southwest China*. Beijing: Geological Publishing House, 1–314 (in Chinese with English abstract).
- Deng Jun, Wang Qingfei, Li Gongjian, Hou Zengqian, Jiang Chengzhu and Leonid Danyushevsky, 2015a. Geology and genesis of the giant Beiya porphyry-skarn gold deposit, northwestern Yangtze Block, China. *Ore Geology Reviews*, 70: 1–27.
- Deng Jun, Wang Qingfei, Li, Gongjian, Hou, Zengqian, Jiang, Chengzhu and Danyushevsky, Leonid, 2015b. Geology and genesis of the giant Beiya porphyry - skarn gold deposit northwestern Yangtze Block China. *Ore Geology Reviews*, 70: 457–485.
- Fu Yu, Sun Xiaoming, Lin Hai, Zhou Haoyang, Li Xin, Ouyang Xianqing, Jiang Liyi, Shi, Guiyong and Liang Yeheng, 2015. Geochronology of the giant Beiya gold-polymetallic deposit in Yunnan Province, Southwest China and its relationship with the petrogenesis of alkaline porphyry. *Ore Geology Reviews*, 71: 138–149.
- Deng Wanming, Huang Xuan and Zhong Dalai, 1998. Petrological characteristics and genesis of Cenozoic alkali-rich porphyry in western Yunnan, China. *Scientia Geological Sinica*, 33(4): 412–425 (in Chinese with English abstract).
- Fu Yu, Sun Xiaoming, Zhou Haoyang, Lin Hai and Yang Tianjian, 2016. In-situ LA-ICP-MS U-Pb geochronology and trace elements analysis of polygenetic titanite from the giant Beiya gold-polymetallic deposit in Yunnan Province, Southwest China. *Ore Geology Reviews*, 77: 43–56.
- Gao Lan, Xiao Keyuan, Cong Yuan, Ding Jianhua, Liu Yaling, Xin Qunye, Wang Shaowen and Hu Guyue, 2016. Metallogenic characteristics and mineral resource potential of the southwestern shanjiang Zn- Pb- Cu- Ag- Sb- Au metallogenic belt. *Acta Geologica Sinica*, 90(7): 1650–1667 (in Chinese with English abstract).
- Ge Liangsheng, Guo Xiaodong, Zou Yilin, Li Zhenhua and Zhang Xiaohui, 2002. Geological characteristics and genesis of Beiya gold deposit Yunnan Province. *Contributions to Geology and Mineral Resources Research*, 17(1): 32–46 (in Chinese with English abstract).
- He Wenyan, 2014. *The Beiya Giant Gold-Polymetallic Deposit: Magmatism and Metallogenic Model*. China University of Geosciences, Beijing (Ph.D. thesis): 1–166 (in Chinese with English abstract).
- He Wenyan, Mo Xuanxue, Yu Xuehui, He Zhonghua, Li Yong, Huang Xingkai and Sun Gangsheng, 2012. Genetic types and the relationship between alkali-rich intrusion and mineralization of Beiya gold-polymetallic ore field, western Yunnan Province. *Acta Petrologica Sinica*, 28(5): 1401–1412 (in Chinese with English abstract).
- He Wenyan, Mo Xuanxue, Yu Xuehui, He Zhonghua and Dong Guochen, 2014. Magmatism and genesis of the Beiya giant gold-polymetallic deposit, SW China. *Acta Geologica Sinica* (English Edition), 88(supp. 2): 83.
- He Wenyan, Mo Xuanxue, He Zhonghua, Noe, C.W., Chen Jinbiao, Yang Kaihui, Wang Rui, Yu Xuehui, Dong Guochen and Huang Xiongfei, 2015. The geology of a mineralogy of the Beiya skarn gold deposit in Yunnan, Southwest China. *Economic Geology*, 110: 1625–1641.
- He Wenyan, Yu Xuehui, Mo Xuanxue, He Zhonghua, Dong Guochen, Liu Xiaobo, Sun Gangsheng and Huang Xiongfei, 2013. Zircon U- Pb and molybdenite Re-Os dating for the Beiya gold-polymetallic deposit in the western Yunnan Province and its geological significance. *Acta Petrologica Sinica*, 29(4): 1301–1310 (in Chinese with English abstract).
- He Zhonghua, Zhou Yunman, He Wenyan, Su Gangsheng, Li Wanhua and Yang Shaowen, 2013. Genetic types and metallogenic regularity of Beiya superlarge gold-polymetallic deposit, northwestern Yunnan. *Mineral Deposits*, 32(2): 244–258 (in Chinese with English abstract).
- He Zhonghua, Yu Degui, Zhou Yunman, Su Gangsheng, Li Wanhua and Chen Jinbiao, 2014. The new knowledge of 5-unification exploration of Beiya super-large gold-polymetallic deposit in Yunnan. *Yunnan Geology*, 33(Supp.): 119–131 (in Chinese with English abstract).
- He Zhonghua, Guan Deren, He Wenyan, Zhou Yunman, Fu Degui, Yang Shaowen, Lu Yongzeng, Wang Lidong, Li Wanhua, Su Gangsheng and Yang Rui, 2016. Exploration model of Beiya superlarge gold-polymetallic deposit, northwestern Yunnan. *Mineral Deposits*, 35(2): 261–282 (in Chinese with English abstract).
- Hoefs, J., 1997. *Stable Isotope Geochemistry*. 4<sup>th</sup> Edition. Berlin Heidelberg: Springer-Verlag, 1–244.
- Hou Zengqian, Zaw, K., Pan Guitang, Mo Xuanxue, Xu Qiang, Hu Yunzhong and Li Xingzhen, 2007. Sanjiang Tethyan metallogenesis in SW China: tectonic setting, metallogenic epochs and deposit types. *Ore Geology Reviews*, 31: 48–87.
- Jia Ruya, Liu Zheng and Liao Shiyong, 2016. Genesis and ore-forming implications of ore-porphyrries from Beiya, western Yunnan. *Mineral Deposits*, 35(Supp.2): 195–196 (in Chinese).
- Jiang Wentao, Li Wenchang, Wang Jianhua, Yin Guanghou, Wu Song, Yu Haijun and Zu Jun, 2015. Geochemical characteristics of PGE and trace element from Beiya gold polymetallic deposit in western Yunnan and their genetic implications. *Acta Mineralogica Sinica*, 35(S1): 430–431 (in Chinese).
- Lai Anqi, Li Zhe, Liu Xuelong and Li Yang, 2016. Petrogenesis and tectonic significance of the Xiuwacu two-period magmatism in Geza arc of Yunnan province: constraints from litho geochemistry, zircon U-Pb geochronology and Hf isotopic compositions. *Acta Geologica Sinica* (English Edition), 90(2): 757–758.
- Li Jun, Ding Jun, Niu Haobin, Ning Guabu, Wang Peng and Ren Fei, 2016. Geochemical characteristics of magnetite from Beiya gold polymetallic deposit in western Yunnan and its constraint on mineralization. *Mineral Deposits*, 35(2): 395–413 (in Chinese with English abstract).
- Li Jinghong, Li Ruliang and Shao Weinian, 1991. The geological characteristic and metallogenesis mechanism of Beiya gold deposit in Heqing, Yunnan. *Southwest Mineral Geology*, 5(2): 50–54 (in Chinese).
- Li Wenchang and Wang Jianhua, 2014. Strike-slip Faults Related Porphyry Gold Deposits on the Western Margin of Yangtze Craton in Southwest China. *Acta Geologica Sinica* (English Edition), 88(supp. 2): 561–562.
- Li Wenchang, Wang Jianhua, He Zhonghua and Dou Song, 2016. Formation of Au-polymetallic ore deposits in alkaline porphyries at Beiya, Yunnan, Southwest China. *Ore Geology Reviews*, 73: 241–252.
- Liu Bo, Liu Huan, Zhang Changqing, Mao Zhihao, Zhou

- Yunman, Huang Hua, He Zhonghua and Su Gangsheng, 2015. Geochemistry and geochronology of porphyries from the Beiya gold-polymetallic orefield, western Yunnan, China. *Ore Geology Reviews*, 69: 360–379.
- Liu Fei, Han Runsheng, Wang Lei, Guo Yuxinyue, Wang Mingzhi and Tan Wei, 2016. Mechanism of rock- and ore-controlling structures in the Wandongshan ore block of the Beiya super-large porphyry-type poly-metallic gold deposit, northwestern Yunnan. *Geotectonica et Metallogenia*, 2016,40(2): 266–280 (in Chinese with English abstract).
- Lu, Y.J., Kerrich, R., Kemp, A.I.S., McCuaig, T.C., Hou, Z.K., Hart, C.J.R., Li, Z.X., Cawood, P.A., Bagas, L., Yang, Z.M., Cliff, J., Belousova, E.A., Jourdan, F., and Evans, N.J., 2013. Intracontinental Eocene–Oligocene porphyry Cu mineral system of Yunnan, Western Yangtze Craton, China: compositional characteristics, sources, and implications for continental collision metallogeny. *Economic Geology*, 108: 1541–1576.
- Ma Deyun and Han Runsheng, 2001. Study on the features of tectono-geo chemistry of Beiya gold deposit and enclosing metallic targets. *Geology and Exploration*, 37(2): 64–68 (in Chinese with English abstract).
- Mao Jingwen, Pirajno Franco, Lehmann Bernd, Luo Maocheng and Berzina Anita, 2014. Distribution of porphyry deposits in the Eurasian continent and their corresponding tectonic settings. *Journal of Asian Earth Sciences*, 79: 576–584.
- Mao Jingwen, Zhou Yunman, Liu Huan, Zhan Changqing, Fu Degui and Liu Bo, 2017. Metallogenic setting and ore genetic model for the Beiya porphyry-skarn polymetallic Au orefield, western Yunnan, China. *Ore Geology Reviews*, 86: 21–34.
- Niu Haobin, Hu Wenyi, Ding Jun, Li Jun, Li Jun, Ning Guabu, Wang Peng, Ren Fei and Dong Li Yang, 2015. Re-Os isotope age of molybdenite in the Beiya gold-polymetallic orefield, western Yunnan, Province and its geological implications. *Geology and Exploration*, 51(1): 1–12 (in Chinese with English abstract).
- Pan Guitang, Xiao Qinghui, Lu Songnian, Den Jinfu, Feng Yimin, Zhang Kexin, Zhang Zhiyong, Wang Fangguo, Xing Guangfu, Hao Guojie and Feng Yanfang, 2009. Subdivision of tectonic units in China. *Geology in China*, 36(1): 1–28 (in Chinese with English abstract).
- Fu Weimin and Hu Chaoping, 1994. On petrology characteristics of alkali-rich porphyry intrusions in Beiya, Heqing and their tectonic environment. *Chinese Geology*, 13 (1): 31–41 (in Chinese with English abstract).
- Ren Zhiji, Luo Rongsheng, Li Lianju, Zhao Chongshun and Li Zhiqun, 2001. Geological characteristics and metallogenic rules of Beiya laterite gold deposit, Yunnan. *Chinese Geology*, 28 (8): 17–22 (in Chinese with English abstract).
- Richards, J.P., and Kerrich, R., 2007. Special paper: adakite-like rocks: their diverse origins and questionable role in metallogenesis. *Economic Geology*, 102(4): 537–576.
- Song Huanbin and He Mingqin, 1994. Secondary ore-forming events of Beiya gold deposit in western Yunnan. *Journal of Kunming Institute of Technology*, 19 (4): 15–20 (in Chinese with English abstract).
- Sun, S.S., and McDonough, W.F., 1989. Chemical isotopic systematics oceanic basalts: Implications for mantle composition processes. In: Saunders, A.D., and Norry M.J (eds.). *Magmatism in the Ocean Basins*. Spec. Publ. Geol. Soc. Lond., 42(1): 313–345.
- Wang Jianhua, Li Wenchang, Wang Keyong, Yin Guanghou, Wu Song, Jiang Wentao, 2015. The characteristics and evolution of the ore-forming fluids in the Beiya porphyry Au polymetallic deposit, northwestern Yunnan. *Acta Petrologica Sinica*, 31(11): 3269–3280 (in Chinese with English abstract).
- Wang Jianhua, Li Wenchang, He Zhonghua, Ying Guanghou and Zhou Yunman, 2016. Geological and Sr-Nd-Pb isotopic characteristics of the Dashadi porphyry in the Beiya gold polymetallic deposit in western Yunnan and their geological implications. *Acta Petrologica Sinica*, 32(8): 2367–2378 (in Chinese with English abstract).
- Wang Mingzhi, Han Runsheng, Wang Lei, Liu Fei, Guo Yuxinyue and Tan Wei, 2016. Tectono-geochemical characteristics of Wandongshan-Bijiashan ore block in the Beiya Au-polymetallic deposit, northwestern Yunnan. *Geology in China*, 43(1): 238–248 (in Chinese with English abstract).
- Wu Kaixing, Hu Ruizhong, Bi Xianwu, Peng Jiantang, Su Wenchao and Chen Long, 2005. Study of the fluid inclusions in altered porphyries the Beiya gold deposit, western Yunnan. *Journal of Mineralogy and Petrology*, 25(2): 20–26 (in Chinese with English abstract).
- Wu Song and Li Wenchang, 2015. The S, Pb isotopic characteristics of layer-like Pb-Zn-Ag Polymetallic deposit of the periphery of Beiya Gold Deposit. *Journal of Mineralogy and Petrology*, 35(S1): 475–476 (in Chinese with English abstract).
- Wyllie, P.J., 1977. Crustal anatexis: an experimental review. *Tectonophysics*, 43(1): 41–71.
- Xiao Qibin, Cai Xinping and Xu Xingwang, 2003. Formation and conservation of Beiya epigenetic deposit, Yunnan Province. *Mineral Deposits*, 22(4): 401–407 (in Chinese with English abstract).
- Xiao Xiaoniu, Yu Xuehui, Mo Xuanxue, Yang Guilai, Li Yong and Huang Xingkai, 2009a. A study of fluid inclusion from Beiya gold-polymetallic deposit in western gold-polymetallic deposit in the western Yunnan Province and its geological significance. *Earth Science Frontiers*, 29(4): 1301–1310 (in Chinese with English abstract).
- Xiao Xiaoniu, Yu Xuehui, Mo Xuanxue, Yang Guilai, Li Yong and Huang Xingkai, 2009b. Geochemistry, zircon SHRIMP U-Pb dating and origin of alkali-rich porphyries in Beiya area, north Erhai Lake, western Yunnan. *Geological Bulletin of China*, 28(12): 1786–1803 (in Chinese with English abstract).
- Xiao Xiaoniu, Yu Xuehui, Mo Xuanxue, Li Yong and Huang Xingkai, 2011. Geochemical characteristics of metallogenesis in the gold-polymetallic deposit in Beiya, western Yunnan Province. *Geology and Exploration*, 47(2): 170–179 (in Chinese with English abstract).
- Xu Shouming, Mo Xuanxue, Zeng Pusheng, Zhang Wenhong, Zhao Haibin and Zhao Handong, 2006. Characteristics and origin of alkali-rich porphyries from Beiya in western Yunnan. *Geoscience*, 20(4): 527–535 (in Chinese with English abstract).
- Xu Xingwang, Cai Xinping, Song Baochang, Zhang Baolin, Ying Hanlong, Xiao Qibin and Wang Jie, 2006. Petrologic chronological and geochemistry characteristics and formation mechanism of alkaline porphyries in the Beiya gold district, western Yunnan. *Acta Petrologica Sinica*, 22(03): 632–642 (in Chinese with English abstract).
- Xu Xingwang, Cai Xinping, Zhang Baolin, Liang Guanghe, Du

- Shijun and Wang Jie, 2007. Genetic types and framework model of Beiya gold ore district in western Yunnan. *Mineral Deposits*, 26(3): 250–264 (in Chinese with English abstract).
- Xu Zhigang, Chen Yuchuan and Wang Denghong, 2008. *The scheme of the classification of the minerogenetic units in China*. Beijing: Geological Publishing house. 1–138 (in Chinese with English abstract).
- Xu Zhiqin, Yang Jingsui, Li Haibing, Ji Shaocheng, Zhang Zeming and Liu Yan, 2011. On the tectonics of the India-Asia collision. *Acta Geological Sinica*, 85(1): 1–33 (in Chinese with English abstract).
- Xue Chuandong, Hou Zengqian, Liu Xing, Yang Zh-ming, Liu Yongqiang and Hao Baiwu, 2008. Petrogenesis and metallogenesis of the Beiya gold polymetallic ore district northwestern Yunnan province, China: Responses to the Indo-Asian collisional processes. *Acta Petrologica Sinica*, 24(3): 459–471 (in Chinese with English abstract).
- Yan Jianguo, Chen Xiansheng and Cui Yinliang, 2002. Search of oreforming process in Beiya gold deposit, Yunnan. *Mineral Deposits*, 21 (Supp.): 743–746 (in Chinese with English abstract).
- Yan Jianguo, Cui Yinliang and Chen Xiansheng, 2003. Metallogenic pronosis and target optimum at Beiya gold deposit in Yunnan Province, China. *Geology and Prospecting*, 39(1): 10–13 (in Chinese with English abstract).
- Yan Mingcai, Chi Qinghua, Gui Tiexin and Wang Chunshu, 1996. Abundance and distribution of chemical elements of igneous in China. *Geochemical*, 25(5): 409–424 (in Chinese with English abstract).
- Yan Qinggao, Jiang Xiaojun, Wu Peng, Sun Huiyi and Guan Shenjin, 2017. Zircon SHRIMP U-Pb geochronology and volcanic edifice division of the Laojiezi intraplate alkali-rich volcanic rocks in Yao'an, central Yunnan province. *Acta Geologica Sinica*, 91(8): 1743–1759 (in Chinese with English abstract).
- Yang Jian, Wang Xuben, Wang Yonghua, Wang Qiao and Zeng Qinqin, 2014. The application of integrated geophysical methods of magnetic survey and AMT to the exploration of the Beiya gold deposit. *Geology in China*, 41(2): 602–610 (in Chinese with English abstract).
- Yang Jian, Tang Fawei, Wang Qiao and Wang Yonghua, 2015. Geochemistry and ore-prospecting targeting in Beiya area, Yunnan Province. *Geology in China*, 42(6): 1989–1999 (in Chinese with English abstract).
- Yang Shiyu and Wang Rixue, 2002. The synthetically information of deposit geological remote sensing of Beiya gold alkali porphyry deposit. *Journal of Kunming University of Science Technology*, 27(4): 1.1–5 (in Chinese with English abstract).
- Ying Hanlong and Cai Xingping, 2004.  $^{40}\text{Ar}$ - $^{39}\text{Ar}$  datings of orthoclase and muscovite from alkali-rich porphyries in the Beiya mine, Yunnan. *Chinese Journal of Geology*, (1): 107–110 (in Chinese with English abstract).
- Yunnan Gold & Mining Group Co. Ltd. 2014. *Report for verification of resource reserves of the Beiya Fe-Au deposit in Heqing County, Yunnan Province*. (5). (Unpublished report)
- Zhang Hongrui and Hou Zengqian, 2015. Pattern and process of continent-continent collision orogeny: A case study of the Tethys collisional orogeny. *Acta Geological Sinica*, 89(9): 1539–1559 (in Chinese with English abstract).
- Zhong Kunming and Yang Shiyu, 2000. The metallogenic prognosis signs of the tectonogeochemistry in Beiya gold deposit Yunnan. *Bulletin of Mineralogy, Petrology and Geochemistry*, 19(4): 393–394 (in Chinese with English abstract).
- Zhou Jiayi, Dou Song, Huang Zhilong, Cui Yinliang, Ye Lin, Li Bo, Gan Ting and Sun Hairui, 2016. Origin of the Luping Pb deposit in the Beiya area, Yunnan Province, SW China: Constraints from geology, isotope geochemistry and geochronology. *Ore Geology Reviews*, 72: 179–190.
- Zhou Yunman, Fu Degui, He Zhonghua, Bao Wei, Li Wanhua and Guan Deren, 2013. The great breakthrough in 5-unification exploration of Beiya gold-polymetallic deposit in Heqing, northwestern Yunnan. In: *Collected works of Yunnan 3-year geological prospecting action plan achievement*. Department of Land and Resources of Yunnan Province, Geological Society of Yunnan, Kunming, 72–82 (in Chinese).
- Zhou Yunman, Fu Degui and He Zhonghua, 2014. The great breakthrough in 5-unification exploration of Beiya gold-polymetallic deposit in Heqing, northwestern Yunnan. *Yunnan Geology*, 33(Supp.): 40–47 (in Chinese with English abstract).
- Zhou Yunman, Wang Lidong, Mei Wenzhou and He Zhonghua, 2015. The questions and measures achieving breakthrough in the unification exploration prospecting. *Southwest Geological Economics*, 189(2): 1–12 (in Chinese).
- Zhou Yunman, Mao Jingwen, Fu Degui, He Zhonghua, Zhang Changqing and Zhao Chengfeng, 2016. *Study on typical deposits and regularity of ore formation in Western Yunnan Province*. Beijing: Geological Publishing House, 394–439.
- Zhou Yunman, Gao Qifang, Liu Zhibin and He Zhonghua, 2017. Occurrence of gold from Beiya gold-polymetallic deposit in northwestern Yunnan province, China. *Acta Mineralogical Sinica*, 37(1/2): 231–245 (in Chinese with English abstract).
- Zhu Xiangping, Mo Xuanxue, White, N.C., Zhang Bo, Sun MingXiang, Wang Shuxiang, Zhao Sili and Yang Yong, 2013. Petrogenesis and metallogenic setting of the Habo porphyry Cu–(Mo–Au) deposit, Yunnan, China. *Journal Asian Earth Science*, 66: 188–203.
- Zou Guangfu, Wang Peng, Niu Haobing, Ren Fei, Ning Guabu, Dong Liyang, Li Jing and Zhou Yexin, 2013. Controlling factors and ore-prospecting targeting in Beiya area, Yunnan Province. *Acta Geological Sinica*, 87(Supp.): 178–182 (in Chinese).

#### About the first author

ZHOU Yunman, male, born in 1965, PhD from China University of Geosciences (Beijing) in 2008, professorate senior engineer, interested in the study of geological mineral resources exploration, mineral deposits and ore prospecting prediction for a long time.